Sub-atomic Species Transport Through Atomically Thin Membranes: Present and Future Applications

Authors: Piran R. Kidambi,[*†§‡] Pavan Chaturvedi[†], Nicole K. Moehring,[§‡]

Affiliations:
[†]Department of Chemical and Bimolecular Engineering, Vanderbilt University, Nashville, TN, USA
[§]Vanderbilt Institute of Nanoscale Sciences and Engineering, Vanderbilt University, Nashville, TN, USA
[‡]Interdisciplinary Graduate Program in Material Science, Vanderbilt University, Nashville, TN, USA
[‡] Department of Mechanical Engineering, Vanderbilt University, Nashville, TN, USA

[*]Corresponding author
Email: piran.kidambi@vanderbilt.edu

Abstract: Atomically thin two-dimensional (2D) materials present opportunities for selective transport of sub-atomic species. The pristine lattice of monolayer graphene and hexagonal boron nitride although impermeable to helium atoms, allow for transmission of electrons, and permit transport of thermal protons and its isotopes. We discuss advances in selective sub-atomic species transport through atomically thin membranes and their potential for transformative advances in energy storage and conversion, isotope separations, in-situ electron microscopy and spectroscopy, and future electronic applications. We outline technological challenges and opportunities for these applications and discuss early adoption in imaging and spectroscopy that are starting to be commercially available, as well as emerging applications in the nuclear industry and future application potential in grid storage, clean/green transportation, environmental remediation, and others.

One Sentence Summary: Sub-atomic Species Transport Through Atomically Thin Membranes.

Main Text: Atomically thin two-dimensional (2D) materials are crystalline solids with constituent atoms bonded in a planar 2D sheet and exhibit distinctly different properties compared to bulk materials(*1*). Graphene, a monolayer mesh of carbon atoms arranged in a hexagonal lattice (~3.4Å thick) was initially isolated as a model 2D-material and can be considered as a building block for other carbon materials such as graphite (stack of graphene sheets held together via van der Waals forces), carbon nanotubes (seamless cylinders of graphene), and buckyballs (seamless spheres of graphene)(*1*). Interest in the properties of 2D-materials have since resulted in successful isolation of monolayers from other layered materials *e.g.* monolayer hexagonal boron nitride (h-BN, isomorph of graphene with alternating B and N atoms), graphene oxide, 2D chalcogenides (~3 atoms thick), 2D oxides, 2D mica (~10Å thick), 2D metal-organic frameworks, 2D covalent-organic frameworks, and others(*2*–*6*), as well as combinations in lateral (in-plane bonding of different 2D-materials) or vertical (stacking different 2D-materials) heterostructures(*2*, *5*).

Membranes are typically thin physical barriers that allow for transport of certain species while hindering others and their ratio is commonly defined as selectivity(*7*, *8*). Monolayer graphene and h-BN represent the thinnest possible physical barrier and allow for selective permeation of

sub-atomic species (Fig. 1), *i.e.* the pristine lattice of graphene and h-BN is impermeable to small atoms such as helium at room temperature(*9*), but allows for transport of protons(*10*) and deuterons(*11*), and shows energy dependent transparency to electrons(*12*). Graphene exhibits excellent thermal conductivity ($(4.84 \pm 0.44) \times 10^3$ to $(5.30 \pm 0.48) \times 10^3$ W/mK)(*13*) and electron mobility (~3,000-230,000 $cm^2V^{-1}s^{-1}$)(*1*, *14*, *15*), while h-BN is an insulator (bandgap ~5.9-6 eV)(*16*) with high thermal conductivity (~751 W/mK at room temperature)(*17*). The exceptional mechanical strength of monolayer graphene (Young's modulus ~1TPa, breaking strength ~42 Nm^{-1})(*18*) and h-BN (Young's modulus ~0.86 TPa, fracture strength of ~70 GPa)(*19*) when suspended over micron scale apertures coupled with the high adhesion energy (graphene ~0.45 Jm^{-2})(*20*) enables the fabrication of functional atomically thin membranes. Monolayer graphene in particular can withstand ~100 bar of applied pressure(*21*) and several orders of magnitude pressure differential(*22*). The pressure tolerance however, depends on the area over which graphene is suspended(*21*) and calculations indicate aperture diameters <1μm are ideal for extreme pressures (up to ~570 bar)(*23*). This review will focus on selective transport of electrons, protons and deuterons through atomically thin membranes and discuss the most promising present and future applications.

Impermeability to atoms, gases and molecules

Graphene and h-BN were initially shown to be impermeable to helium and other gases (Fig. 1C inset)(*9*, *20*). Atomically thin balloons formed by sealing micron-sized gas-filled cavities with mechanically-exfoliated monolayer graphene or h-BN flakes exhibited negligible leakage (transport of gas through the 2D lattice) rates indicating their lattice is impermeable to helium and larger atoms/molecules at room temperature(*9*, *24*, *25*) and monolayer molybdenum-di-sulfide (MoS_2) is impermeable to H_2 at ~50 °C (1 bar and over 3 days)(*26*). In contrast, high gas leakage rates were observed for even nanoscale defects(*24*, *25*, *27*). Theoretical calculations were in agreement with experimental observations of gas impermeability and predicted large energy barriers (E_B) for the permeation of atoms through the hexagonal rings (radius ~1.42-1.45Å) in the pristine lattice of graphene (H atoms E_B ~2.86-4.61 eV, He atoms E_B ~3.5-18.77 eV, O atoms E_B ~5.5 eV and N atoms E_B ~3.2 eV) and h-BN (H atoms E_B ~6.38 eV)(*9*, *28–31*).

The impermeability of graphene and h-BN to even small gas atoms at room temperature offers routes to create atomically thin barriers or atomically sharp interfaces separating two distinct reservoirs of atoms/molecules. However, observations of anomalous H_2 permeation through monolayer graphene, while maintaining impermeability to the smaller helium atoms as well as the absence of molecular deuterium (D_2) permeation(*26*), taken together with the stochastic switching behavior of leakage rates observed in some atomically thin balloon experiments(*24*, *27*, *32*), raises fundamentally interesting questions on the absolute limits of gas impermeability, as well as the transport mechanisms (and associated E_B) for selective H_2 permeation(*26*).

In contrast, the transmission of energetic He ions/alpha particles and other larger ions through graphene, h-BN and other 2D-materials depends on the ion energy, size, and incident angle wherein collisions with the 2D lattice can also result in the formation of defects with varying yields(*33*, *34*). Irradiation with energetic ions, protons, as well as alpha, beta, and gamma particles, is typically used to assess the reliability of electronic devices incorporating 2D-materials for space applications(*35*, *36*). Finally, selective transport of atoms, molecules and ions, through defects in 2D-materials presents potential for advancing separation processes(*7*, *8*).

Transmission of electrons

Electron transmission through 2D-materials entails combinations of electron-electron and electron-phonon interactions in the lattice, via elastic and inelastic collisions with the nuclei of the atoms in the lattice(*37*). Electrons tunnel through the lattice of monolayer graphene(*38–40*) and h-BN (tunnel-barrier height ~3.07 eV, dielectric strength ~7.94 MV/cm)(*41*, *42*), and the in-plane electron conductivity of graphene can be used to modulate tunnelling via changes to the potential or charge distribution, the tunnelling electrons encounter during transport in the normal direction(*39*). In this context, emerging electronics applications such as the use of graphene and h-BN as tunnel-barriers for spintronic devices,(*43*) as well as vertical transistors exploiting electron tunneling(*39*, *42*, *44*) show promise.

The transmission of energic electrons through graphene varies with their kinetic energy (Fig. 1A). For low energy electrons (~40–200 eV) simulations predict transmission >80% through monolayer graphene,(*45*) that appear to be in agreement with experimentally measured transmission coefficients (ratio of transmitted electron current (I_0) to incident electron current(I)) of ~0.6-0.74 for electrons with ~2-205 eV kinetic energy(*46–48*). For electrons with kinetic energy ~200-1600 eV, the measured transmission coefficients for monolayer graphene increases with electron kinetic energy (Fig. 1A)(*12*, *49*). The electron attenuation lengths ($\lambda_{EAL} = d_G/\ln(I_0/I)\cos\theta$) computed from the measured transmission coefficients I_0/I (assuming graphene thickness d_G ~3.35Å and incident angle ($\theta = 0$), show reasonable agreement with values computed using the inelastic mean free path predictive formula (TPP-2M model) for graphite(*50*), and deviations at lower energy were ascribed to elastic scattering(*12*). These theoretical and experimental observations suggest the inelastic mean free path of electrons provides a reasonable measure of the electron transparency of graphene indicating its potential as an electron transparent gas impermeable barrier for electron microscopy and spectroscopy(*12*, *51*). Electron transmission decreases with increasing number of graphene layers(*12*) and therefore bulk graphite is expected to show significantly lower electron transmission.

Graphene and h-BN show reasonable tolerance to irradiation induced damage from electron beams ~60-80keV even for high beam doses under vacuum(*37*, *52*). At electron energies >80keV, knock-on damage with ejection of atoms from the lattice is observed for monolayer graphene with formation of structural/vacancy defects as well as defect clusters in the lattice upon prolonged irradiation(*52*). Graphene synthesized using C^{13} isotope shows a slightly higher threshold >95keV for knock-on damage.(*52*) For monolayer h-BN, irradiation with electron beam ~80keV results in preferential ejection of B atoms and the metastable nitrogen terminated zig-zag edges preserve a triangular vacancy defect shape(*53*, *54*). However, the electron irradiation tolerance at higher pressures for graphene(*55*) and h-BN(*56*) depends on the gas composition of the environment with the possibility of beam-induced reactive chemical degradation/etching(*57*).

Permeation of protons and deuterons

The impermeability to helium atoms and electron transparency of the pristine graphene and h-BN lattice raised fundamentally important scientific questions regarding the transport of protons. Protons represent an interesting intermediate case(*10*), and theoretical/experimental understanding of transport is still emerging.

Initially, permeation of protons through the pristine graphene lattice was assessed to be improbable based on calculated energy barriers (E_B) ~1.41-2.21 eV and transport was hypothesized to only occur in the presence of lattice defects which reduce the barrier height(*29*). However, areal conductivity ~3 $mScm^{-2}$ for graphene (E_B ~0.78± 0.03 eV) and ~100 $mScm^{-2}$ for h-BN (E_B ~0.3 ± 0.02 eV) were measured at room temperature during electric-field-driven transport of thermal protons through micron-scale mechanically-exfoliated flakes sandwiched between Nafion, an ionomer that conducts protons in the hydrated state (Fig. 2A,B)(*10*). Since Nafion shows negligible electron conductivity, the current obtained was a measure of proton transport through the graphene and h-BN lattice(*10*). Nafion sandwich devices with monolayer MoS_2 did not show measurable proton current under similar experimental conditions(*10*). The measured increase in proton conductivity with temperature (Arrhenius dependence) indicated values >1 Scm^{-2}, required for practical energy relevant applications, could be attained at relatively mild temperatures for h-BN (>80 °C) and graphene (>110 °C)(*10*).

The large difference in proton conductivity for graphene and h-BN despite only ~1.8% lattice mismatch(*40*), is attributed to the polar nature of bonds in h-BN which results in valence electrons concentrating around the N atom, leading to larger openings/pores in the electron cloud for the h-BN lattice compared to graphene (Fig. 1B inset)(*10*). The proton conductivity decreases with increasing number of layers due to an increase in integrated electron density *i.e.* bilayer h-BN (~5 $mScm^{-2}$) and tri-layer h-BN (~0.1 $mScm^{-2}$), while bilayer graphene shows negligible transport(*10*). Differences between bilayer graphene and h-BN are attributed to different stacking order *i.e.* the AA' stacking in h-BN aligns the hexagonal rings between different layers preserving the central pore, while the AB stacking in graphene positions a carbon atom in one layer in the center of the hexagonal ring in the next layer, effectively blocking the pores in the electron cloud(*10*). Bulk graphite and h-BN are hence expected to be impermeable to protons.

Proton conductivity similar to Nafion sandwich devices were also measured for micron-scale mechanically-exfoliated graphene (~3 $mScm^{-2}$) and h-BN (~100 $mScm^{-2}$) separating liquid electrolytes (0.1M HCl, Fig. 2A)(*10*, *25*). The areal conductivity showed a linear dependence on the electrolyte concentration *i.e.* at 1M HCl ~1 Scm^{-2} for monolayer h-BN, and ~12 $mScm^{-2}$ for monolayer graphene were measured (Fig. 2B), indicating the concentration of protons interfacing the 2D lattice could influence transport rates(*25*). A Nernst analysis of membrane potentials showed that protons account for nearly all the observed currents with no detectable flow of counter ions (Cl^-) indicating near perfect proton selectivity(*25*). Although these studies implemented rigorous controls and measured negligible gas leakage rates through the membranes compared to noticeable gas fluxes for graphene synthesized via chemical vapor deposition (CVD) with intrinsic defects(*10*, *25*), some studies attribute proton transport through CVD graphene in the liquid-phase to atomic scale defects in the lattice(*58*, *59*). Further research is expected to improve fundamental understanding and shed light on the origins of these differences.

The deposition of a discontinuous layer of Pt on the 2D lattice to form Nafion-2D-material-Pt devices (where protons permeating the 2D lattice recombine on Pt to evolve H_2 gas, Fig. 2A) further increased proton conductivity of graphene to ~90 $mScm^{-2}$ (reducing E_B by ~0.5 eV) while ~3 Scm^{-2} was measured as a lower bound for h-BN (Nafion resistance limited proton current)(*10*, *60*). Although the attraction of transient protons to Pt has been suggested to play a role(*10*, *60*), further research may provide mechanistic insights. Illuminating the Nafion-graphene-Pt devices with visible light (100 $mWcm^{-2}$) resulted in further increase in proton

conductivity to ~20 Scm^{-2} (at ~2.8V) and up to 10× higher proton fluxes than for devices in the dark(*60*). The measured gain of ~10^4 protons per photon (photo-responsivity ~10^4 AW^{-1}) and response times in the microsecond range can possibly enable photodetector applications(*60*). Similar effects, are also seen for Pd and Ni nanoparticles (albeit not as effective as Pt) that also strongly interact and n-dope graphene, and the observed effects are attributed to photovoltages created from hot electrons generated in graphene (upon illumination of in-plane electric fields/built-in junctions formed in areas surrounding the nanoparticle due to n-doping) that funnel protons and electrons towards the metal nanoparticle resulting in enhanced rate of electron–proton conversion to atomic hydrogen on the nanoparticle(*60*).

Theoretical studies have proposed different mechanisms (via hydrogenation/protonation) and transport pathways (straight perpendicular path through the center of the hexagonal ring, E_B ~1.41 eV or via chemisorption, E_B ~2.21 eV) to explain the measured proton conductivity for graphene and h-BN (Fig. 2C)(*29*). While the computational methods vary, most studies computed E_B >1.4 eV for graphene,(*28*, *29*, *59*, *61–65*) and E_B >0.9 eV for h-BN(*31*) and the inclusion of quantum effects such as tunneling and zero-point energy can further reduce E_B by ~0.5 eV(*61*) bringing the theoretical values (Fig. 2D) closer to the experimentally measured values E_B ~0.8 eV (graphene) and E_B ~0.3 eV (h-BN)(*10*). Theoretical studies of proton transport in the presence of water molecules *i.e.* proton transfer from H_3O^+ on one side to H_2O on the other (comparable to experimental approaches interfacing 2D crystals with hydrated Nafion or aqueous electrolytes) suggest that hydrogenation of graphene reduces E_B from >3 eV to <1 eV(*62*). E_B ~1eV for proton transport through multi-protonated graphene was also computed for a co-operative mechanism where nearby chemisorbed protons facilitate chemisorption of subsequent protons onto a carbon atom in the hexagonal ring, followed by bond-flipping via the C-C bond to allow for proton transfer to the other side (Fig. 2C)(*64*).

In addition to proton transport, transport of the heavier isotope deuteron was also measured through pristine monolayer flakes of graphene and h-BN using Nafion-2D-material-Nafion devices (Fig. 2A)(*11*). The rate of transport for deuterons were an order of magnitude lower than protons allowing for a separation factor or selectivity ~10 ($10H^+$:$1D^+$) arising due to difference in vibrational zero-point energies (~60meV) of transient protons and deuterons bound to the SO_3^- groups in the Nafion before being incident on the graphene or h-BN lattice(*11*).

While the measured areal proton conductivity for pristine graphene (~3 $mScm^{-2}$) and h-BN (~100 $mScm^{-2}$) at ambient temperature are lower than state-of-the-art industry standard ionomers such as Nafion (thickness dependent proton conductivity ranging from ~1-20 Scm^{-2}, Fig. 2B)(*10*, *66*), atomic scale defects in the lattice as well as domain boundaries in CVD graphene have been shown to increase proton conductivity to ~29 Scm^{-2} (after subtracting Nafion resistance) while maintaining negligible transport of K^+ in Nafion-graphene-Nafion devices(*66*). Despite the presence of defects in CVD graphene, a H^+/D^+ isotope selectivity ~14 ($14H^+$:$1D^+$) was maintained(*66*), indicating that the mere presence of defects alone did not change the dominant mode of rate based H^+/D^+ isotope separation in these devices(*66*, *67*).

Theoretical calculations for H^+ and D^+ transport through topological Stone–Wales defects (55-77SW) predict energy barrier <1 eV and H^+/D^+ selectivity ~7 at ambient conditions(*68*). These calculations offer an alternative interpretation with proton transport occurring primarily through defects in the 2D lattice rather than permeation through the pristine lattice. Such an interpretation would be consistent with proton conductivity along with negligible gas leakage rates measured for mechanically-exfoliated graphene and h-BN(*10*, *25*), very high proton conductivity along

with high H^+/D^+ selectivity for CVD graphene with grain boundaries(*66*, *67*) containing pentagon-heptagon rings(*69*), as well as the high proton conductivity ~1 Scm^{-2} for nanocrystalline graphene (NG) and monolayer amorphous carbon (MAC, with eight carbon atom rings) along with negligible gas leakage rates(*4*, *70*).

Practical applications will require large-area 2D-materials synthesized via scalable approaches such as CVD that inevitably introduce intrinsic defects, grain boundaries, wrinkles, and other defects (Fig. 3) and the proton transport properties may be quite different than pristine 2D-material (Fig. 2B)(*58*, *59*, *66*, *67*, *71–74*). Hence, understanding selective proton transport behavior of CVD grown 2D-materials is imperative for advancing applications. Notably, nanoscale defects introduced in CVD graphene via ion-beam bombardment,(*74*) plasma treatments, and incorporating dopants can increase ionic conductance(*74*, *75*) with pH dependence confirming protons as the main contributors(*74*). However, non-selective defects can also increase ionic conductivity with loss in proton selectivity. Finally, the emergence of new materials such as 2D mica (~10Å in thickness and ~5Å wide tubular channels) that exhibit 1-2 orders of magnitude higher proton conductivity (~100 S cm^{-2} at 500 °C) than graphene or h-BN have ignited research interest in ultra-thin membranes that could operate under high temperatures increasing the efficiency of fuel-cells and as well as under dry/un-hydrated conditions.(*4*) Other 2D-materials *e.g.* Phosphorene (E_B ~0.48) and Silicene (E_B ~0.12) have been explored theoretically(*31*) for enhanced proton transport but their limited stability under ambient conditions presents challenges.

Advances in Synthesis and Processing of Atomically Thin Membranes

Mechanical exfoliation was initially used to isolate monolayers of 2D-materials and suspend them over apertures to form atomically thin membranes (Fig. 3)(*1*, *9*, *20*). Although it produces the highest quality of pristine flakes ideally suited for probing fundamental material and transport properties, the flake sizes remains limited to a few microns(*9*, *10*, *24–27*). Practical membrane applications will require scalability over much larger areas and will need higher levels of homogeneity in terms of layer numbers, film coverage and quality(*8*). While liquid phase exfoliation of 2D-materials allows for scalability, fabricating atomically thin membranes from randomly oriented collage of flakes of multiple sizes, shapes and thicknesses is inherently challenging(*8*, *76*). Bottom-up synthesis via CVD (using a catalytic substrate to dissociate a precursor vapor followed by self-assembly via nucleation and subsequent growth at elevated temperatures) and its variants allow for continuous monolayer films of graphene(*77*), h-BN(*78*), nanocrystalline graphene(*79*), monolayer amorphous carbon(*80*), and other 2D-materials(*81*) where the scalability is in-principle only limited by the catalyst/substrate surface area and reactor design(*82*), *e.g.* synthesis of ~10×10cm monolayer h-BN(*83*) and ~100m of monolayer graphene via roll-to-roll processes(*84*) have been demonstrated. However, CVD grown monolayers are typically polycrystalline with domain boundaries(*69*) as well as intrinsic defects within the domains that could allow for non-selective leakage (Fig. 3)(*85*).

Efforts towards improving the quality of CVD grown 2D-materials were largely driven by requirements for electronic applications *i.e.* minimizing electron scattering at grain boundaries to achieve performance comparable to mechanically-exfoliated flakes(*86*). Hence, increasing domain sizes within the polycrystalline film has been the primary focus with the ultimate goal of producing single crystalline 2D-materials without grain boundaries via three main approaches

(Fig. 3). In the first approach, a single crystalline substrate is used to nucleate domains of 2D-material that align with respect to each other and orient in the most energetically favourable crystallographic direction with respect to the substrate(*83*, *87*, *88*) or electrostatic interaction between domains is used to achieve alignment on a liquid metal(*89*). Such alignment results in seamless merging of the individual domains into a continuous film without domain boundaries(*83*, *87–89*). In practice, single crystal substrates are expensive to produce and ensuring perfect alignment of all domains with respect to each other is non-trivial since a small fraction of unaligned domains can result in polycrystalline films(*87*). In the second approach a single nucleus of the 2D-material is grown larger in size without the nucleation of additional domains by carefully controlling the supply of precursor(*90*), but the processing is typically long *i.e.* few hours compared to processes that require a few minutes or seconds(*91*). Thirdly, an approach of evolutionary selection in which multiple domains nucleate but careful control of gas supply through a nozzle on a moving substate results in one nuclei outgrowing the others(*92*). This method allows for the use of in-expensive polycrystalline catalyst foils to produce single crystalline monolayer 2D-materials via kinetic control(*92*) and is adaptable to roll-to-roll CVD offering process scalability(*82*, *84*).

However, single crystalline 2D-materials are still not completely devoid of defects including vacancy defects(*8*, *93*), and the quality requirement for membrane applications tend to be somewhat different than electronic applications(*7*, *8*, *94*). For example, intrinsic defects (*e.g.* Stone Wales 55-77) and grain boundaries can allow for enhanced proton transport(*66*, *68*), but larger defect sizes could result in leakage of gases, ions and larger molecules compromising selectivity(*7*, *8*, *24*, *25*, *27*). Additionally, nanoscale defects show a propensity to cluster along wrinkles originating from differences in thermal expansion coefficients between the 2D-material and catalyst, and the detrimental effects of leakage (loss in selectivity) through even a very small number of nanoscale defects is greatly exacerbated for atomically thin membranes applications compared to most electronic applications(*94*). In this context, recent synthesis of nanocrystalline graphene(*79*), and monolayer amorphous carbon(*80*) show promise but attaining atomic scale control and complete absence of larger defects over large areas remains non-trivial, necessitating leakage sealing approaches(*95*, *96*), while large-area synthesis of 2D mica remains to be demonstrated(*4*).

In addition to synthesis, the interfacing of the 2D-material by transferring it from the growth substrate to an appropriate support is crucial to enable membranes applications (Fig. 3B)(*7*, *8*). Transfer procedures developed for 2D-materials device fabrication *e.g.* sacrificial polymer scaffolds(*9*, *24–27*, *83*, *87*, *88*) or the use of an evaporating solvent to adhere 2D-materials to TEM grids(*97*) can aid small area membrane (few microns to centi-meter scale) fabrication while scalable approaches such as hot-pressing(*66*), polymer support casting(*98*) and roll-to-roll lamination(*99*) along with approaches for effective re-use of the catalyst(*100*) may enable scalable, cost-effective synthesis of atomically thin membranes for large area (centi-meter to meter scale) applications(*7*, *8*). Leveraging synergistic opportunities such as roll-to-roll processes for 2D-material synthesis as well as membrane fabrication may provide rapid advances in this area(*8*, *82*, *99*).

Commercial production of large-area 2D-materials is slowly maturing. While polycrystalline centi-meter scale CVD graphene has been available commercially for almost a decade, innovations in processing and economies of scale have allowed for cost of bulk orders of CVD graphene on Cu foil to steadily drop from ~ €1,000/cm^2 in 2010 to ~ €2/cm^2 indicating that

applications using small areas of graphene can already be cost competitive while delivering improved functionality(*101*, *102*). Based on the current trends, a further reduction in price for graphene may be expected and translating learnings from developments with graphene can perhaps aid compressed timescale for commercial production of other 2D-materials.

Applications of selective proton transport through atomically thin membranes

Selective proton transport through atomically thin membranes along with impermeability to atoms, gases and hydrated ions presents opportunities to improve efficiencies across a wide spectrum of energy generation and conversion processes in the hydrogen economy as well as enabling additional separation processes (Fig. 4).

Fuel-cells and hydrogen pumps: Fuel-cells powered by renewably generated hydrogen or methanol/ethanol are expected to play an important role in environmentally sustainable advances towards clean/green transportation, distributed and mobile auxiliary power generation (Fig. 4)(*103*). Nafion and sulfonated polyether ether ketone (S-PEEK) currently represent the most widely used fuel-cell membranes but suffer from cross-over of reactants (leakage of undesired species through the membrane thereby reducing selectivity), swelling/softening at high relative humidity and require hydrated environments for proton conductance(*104*, *105*). Hydration requirements also limit the maximum operating temperatures hindering efficiency gains(*103–107*).

Among the many approaches to improve the operability of proton conducting polymers(*108*), coating continuous layers of graphene or h-BN has been shown to limit cross-over of hydrogen(*109*) or methanol in fuel cells(*110*, *111*). In hydrogen fuel-cells, the effect was more pronounced in accelerated stress tests for ~100 hrs *i.e.* H_2 permeation currents (measured at 0.4V, 30% relative humidity and 90°C) for 1 or 3 layers (AA' stacked) h-BN-coated-Nafion showed almost no change compared to >100× increase for bare Nafion, indicating long-term benefits(*109*). In the case of methanol fuel-cells, decrease in cross-over up to ~68% is observed for monolayer graphene coated Nafion compared to bare Nafion, allowing higher concentrations of methanol (up to ~10M compared to typical 1-5M) to obtain enhanced power density(*111*).

The reduction in cross-over can however come at the expense of low proton conductivity of 2D-materials that can decrease the overall efficiency of the fuel-cell by increasing the ohmic losses(*109–111*). Higher operating temperatures(*110*, *111*) or the incorporation of selective defects in the 2D lattice can enhance proton transport(*66*, *74*). However, achieving atomic precision in defect sizes over large-area membranes using scalable processes remains non-trivial and leakage sealing techniques(*7*, *8*, *96*) as well as appropriate support selection(*112*) could play a crucial role in increasing functionality by minimizing non-selective leakage. h-BN and graphene membranes supported on porous polymers or even ceramics can allow for membranes with high proton selectivity that can operate in anhydrous environments and medium temperatures 110–160°C (h-BN is stable up to ~500-700°C in air(*113*)) aiding increased fuel-cell efficiencies as well as their possible use in other kinds of fuel-cells(*103*, *104*, *106*, *107*).

Although Li-ion battery (specific energy >250Whkg^{-1}) vehicles currently have a higher market penetration for passenger vehicles and will continue to in the near future due to established electricity infrastructure (despite relatively long charging times), the extra weight required to enhance the range of fuel-cell vehicles is negligible compared to drastic weight compounding for

battery powered vehicles(*106*, *107*, *114*). These differences are exacerbated in the context of clean/green cargo and commercial transport both on land via heavy vehicles/trucks/buses and on shipping routes(*106*, *107*, *114*). Hydrogen fuel-cell powered vehicles have also been under development for under-water transport systems and military applications where the longer ranges from high energy density of H_2 (~120-142MJ/kg) as well as low thermal and acoustic signatures allow for extended periods of quiet submergence and undetected transport(*107*). Finally, the use of hydrogen fuel-cells for aviation are also under consideration, particularly for unmanned ariel vehicles(*107*). The already high cost of Nafion membranes ($75-250/kg ionomer cost for high-volume manufacturing)(*115*) accounts for ~9-17% of the fuel-cell cost(*107*) and the addition of 2D-materials is likely to increase costs further. However, advantages in increased efficiency over the targeted membrane life-cycle of operation *i.e.* ~40,000 hours (stationary fuel-cells) and ~5,000 hours (transportation fuel-cells)(*116*), need to be considered during feasibility analysis. Studies are also needed to evaluate long-term durability and chemical stability of 2D-materials under real-world fuel-cell operating conditions.

The lack of hydrogen infrastructure perhaps presents the most severe challenge to the hydrogen economy(*103*, *106*, *107*, *114*). Leveraging the potential of agricultural waste in rural areas, waste water and industrial waste in urban areas to generate biogas/methane (and H_2 via reforming, predicted total capacity of USA ~2.8 million tonnes and enough to power ~11 million fuel-cell vehicles per year) as well as the use of existing natural gas infrastructure are some viable approaches for possible distributed H_2 production (Fig. 4A)(*117*). Separating H_2 from reformate mixtures can allow for carbon capture (which can further be converted into economic value organic molecules such as methanol, formic acid, olefins etc) or carbon storage for negative carbon emissions technologies, particularly for H_2 sourced from biogas generated from waste streams(*117*). Here, compact separators using electrochemical hydrogen pumps can aid distributed H_2 production(*107*). Electrochemical hydrogen pumps incorporating proton selective atomically thin membranes can allow for facile, compact, single-step H_2 separation and purification (>99.97% purity needed for fuel-cells) alleviating the need for multi-stage conventional separation processes(*116*). In addition to separation from reformate mixtures, such proton pumps can also be used to pump against a pressure gradient to allow for a single-step purification and pressurization of H_2 and facilitate dispensing for fuel-cells.

Redox flow batteries and grid storage: Grid scale energy storage is emerging as a critical requirement for future electricity grids powered by periodic and/or intermittent renewable energy such as solar and wind (Fig. 4). Redox flow batteries, where ions in electrolyte solutions undergo a change in the redox states via the exchange of protons through a cation conducting polymer separating two reservoirs, are emerging as promising technology platforms(*118*). Vanadium redox flow batteries in particular, offer distinct advantages with scalability in storage capacity from stand-alone units ~few kW to 200 MW (under construction)(*119*), thousands of deep-discharge cycles (>15,000), >20 years of life-time, are non-flammable and allow for independent control of power and energy storage(*118*, *120*, *121*). Nafion, S-PEEK and other proton conducting polymers are the current industry standard for vanadium flow batteries but do not offer high selectivity between protons and vanadium ions and thereby suffer from crossover of vanadium ions as well as other undesired redox species leading to long-term efficiency losses(*118*, *120*, *121*). Sandwiching monolayer graphene or h-BN between layers of Nafion or S-PEEK has been shown to increase proton selectivity(*120–122*). In particular for CVD graphene sandwiched between Nafion, proton transport ($0.02 \pm 0.005\ \Omega\ cm^2$) four orders of magnitude faster than vanadium ion transport ($223 \pm 4\ \Omega\ cm^2$) and near complete elimination of crossover

was observed under lab scale test conditions(*121*). The chemical robustness of graphene or h-BN to highly acidic electrolyte environments coupled with selective proton transport presents potential for advancing new kinds of proton exchange membranes by using inert polymers *e.g.* Teflon to support the 2D-material, although long-term studies under realistic operating conditions are required to evaluate durability and stability.

Isotope separation and nuclear technologies: Isotopes of hydrogen (hydrogen H, deuterium D, and tritium T) are widely used for nuclear, military, medical and research applications(*67*). Conventional H^+/D^+ separation processes for heavy-water production (D_2O, used as a moderator for neutrons as well as a coolant in nuclear reactors) are extremely energy intensive requiring multi-stage separations due to poor selectivity *e.g.* Girdler-Sulfide process (H^+/D^+~1.3) and monothermal-NH_3/H_2 process (H^+/D^+~6)(*67*, *123*, *124*). The naturally occurring low concentration of D ~0.015% in water coupled with the low selectivity of conventional processes, necessitates processing of enormous quantities to produce ~1Kg D_2O with an energy consumption ~10 MWh, thereby increasing capital and operating costs(*67*, *123*, *124*).

Here, selective H^+ and D^+ transport through graphene and h-BN with rate-based separations factors $H^+/D^+ \geq 10$ offers transformational advances(*11*, *66*). Large-area electrochemical proton pumps with monolayer CVD graphene show selectivity H^+/D^+~8 despite the presence of cracks and defects as well as ~1-2 orders of magnitude reduction in energy consumption compared to current technologies(*67*). Extrapolating the measured flux ~0.8 mmol h^{-1} cm^{-2} at 0.5V in the electrochemical pumps indicates a graphene membrane ~30 m^2 would produce ~40 tons of heavy-water per year comparable to that of a modern plant(*67*), and h-BN is expected to offer even higher performance. Similar advantages for removal of radioactive tritium (T) from contaminated water in commercial and research nuclear reactors are predicted with higher selectivity H^+/T^+ ~37(*11*, *65–67*). Finally, such technologies are expected to be leveraged to supply experimental fusion reactors that require T as a fuel(*125*) as well as separating mixtures of T-^{3}He to recover ^{3}He for applications in radiation monitors for border security at ports of entry to detect illicit transport of radiological or nuclear materials(*126*).

Applications for the electron transparency of atomically thin membranes

The energy dependent electron transparency of graphene along with its atomic-thinness, electrical conductivity, excellent mechanical strength and impermeability to gases offers transformative opportunities for advancing electron microscopy and spectroscopy(*49*, *57*, *97*, *127–129*), as well as extending conventional in-situ metrology techniques requiring high-vacuum environments to new frontiers (Fig. 5) such as ambient pressures(*6*, *49*), liquid systems(*12*, *129*, *130*), and biology(*127*, *131*).

Atomically thin substrates for transmission electron microscopy (TEM)

Graphene represents the ideal substrate material to support samples for TEM imaging, and offers distinct advantages over the typically used ~3-20nm thick holey amorphous carbon films.(*57*) The electron transparency of atomically thin graphene (~0.34nm) at acceleration voltages typically used in TEM, minimizes background noise and contributions at high-resolution can be effectively filtered out using the periodicity of the crystalline lattice(*37*, *57*, *132*). The high mechanical strength and chemical inertness of graphene (compared to amorphous carbon), along with its ability to maintain integrity under ~80keV electron beams (even at high beam dose) and

effective charge dissipation, have enabled advancements in imaging individual low-atomic-number atoms and adsorbates, 1D materials such as CNTs and nanowires, 2D-materials and heterostructures, organic compounds/molecules, biological materials and biomolecules, nanoparticles and clusters supported on graphene, including their dynamic interactions with graphene and between themselves(*57*, *132*, *133*). The uniform thickness of monolayer graphene and opportunities for chemical modification of its surface (for enhanced interaction with biological specimens) presents advantages for sample preparation for cryogenic electron microscopy of biological samples by enabling the formation of uniform ice thicknesses along with minimal signal from graphene used as a sample support(*134*, *135*). The use of graphene for TEM grid supports (aided by small areas required ~few mm^2(*134*) and high transfer yields(*135*)) was one of the first application to progress successfully into the commercial arena(*102*) with several companies *e.g.* Ted Pella Inc., ACS materials, etc., offering graphene coated TEM grids in their product line. However, electron beam induced knock-on damage >80keV and limited chemical/thermal stability compared to silicon nitride (SiN_x) present some limitations but these may be mitigated to some extent by advances in aberration correctors that allow for high resolution imaging <80keV(*37*, *57*).

Electron transparent windows for in-situ electron microscopy and spectroscopy

The use of graphene as an atomically thin electron transparent barrier (replacing the typically used ~15-50nm thick SiN_x membranes with high atomic number Z and electron-scattering(*130*)) to isolate the sample environment from the vacuum environment of analyzers/detectors (Fig. 5), presents transformative opportunities for advancing in-situ electron microscopy and spectroscopy(*12*, *49*, *129*, *136*). The simplest configuration involves covering the sample with a layer or two (where defects in the 1st layer are sealed by the 2nd layer) of graphene (Fig. 5A,D,E). Since the characteristic mean free path of the generated secondary/photo electrons is typically larger than graphene thickness, such an approach allows for probing the top few nanometres of the sample surface via photoelectron spectroscopy (PES) and microscopy(*12*, *49*, *137*) and scanning electron microscopy (SEM)(*136*, *138*). Such approaches have enabled PES of wet and gaseous samples (Fig. 5D)(*12*, *136*, *137*), up to ~1-1.5bar pressure (Fig. 5E)(*22*), as well as SEM imaging of live bacterial cells without labels (Fig. 5A)(*138*). In the latter, graphene's impermeability protected the cells from the vacuum environment, while the scavenging of radicals (generated due to radiolysis of water by the e-beam) by graphene along with its electrical conductivity allowed for 100-fold increase in electron dose after which the cells still appear to maintain structure and function(*138*). An alternative approach in airSEM(*131*), seals the electron optics in an SEM with graphene and uses the mean free path of electrons in air ~10-100μm to enable high contrast imaging and improved spatial resolution (at 7 kV acceleration voltage, simulated electron scattering from bilayer graphene is ~3% compared to ~75% for 10 nm SiN_x membrane) under ambient conditions eliminating the need for a specimen vacuum chamber (Fig. 5B)(*131*). A third configuration isolates the sample (usually a liquid solution or biological samples) between two graphene layers and allows for atomic resolution TEM of nanoparticles in liquids (and their growth and dynamics)(*97*, *129*) as well as nm resolution electron energy loss spectroscopy of biomolecules(*127*). Although early approaches used static solutions in hermetically sealed graphene pouches (Fig. 5C) limiting studies to e-beam induced or time lapsed studies,(*97*) systematic advances have resulted in the development of multi-channel arrays capped with graphene (Fig. 5D) and complete flow cells with graphene windows that allow for in-situ and in-operando studies on a range of material including biological systems(*129*). Similar advances are also seen for PES and SEM with combinatorial studies being

made possible (Fig. 5D)(*128*). Taken together, graphene windows present potential for transformational insights into reaction mechanisms at the solid-liquid interface, heterogeneous catalysis under realistic pressures, crystal nucleation/growth/dissolution, material performance in batteries, biological processes and others that have previously remained inaccessible(*12*, *49*, *127*, *129*, *130*, *136–138*). Finally, the electrical conductivity of graphene enables its use as a model electrode, facilitating fundamental understanding of electrochemical processes in-operando (Fig. 5D)(*137*). Despite these advantages, issues regarding bubble formation due to radiolysis of water by the e-beam (which can alter solution pH and concentrations of electrolytes), mechanical integrity of graphene membranes (damage to the graphene from bubble collapse or attack from free radicals), perturbations/damage to the interface being probed and any influence from the graphene surface or residual contaminants on the graphene surface are issues that still need to be addressed(*12*, *129*, *130*, *136–138*).

Outlook

Electron, proton and deuteron permeation through atomically thin graphene and h-BN presents potential for break-through advances in several fields. However, fundamental understanding of transport mechanisms is still emerging and advances in measurement techniques/resolution are furthering insights *e.g.* anomalous H_2 transport through graphene (proposed to occur via H_2 dissociation on catalytic ripples/wrinkles and subsequent flipping of adsorbed atoms to the other side of the 2D lattice)(*26*) has renewed focus on the limits of gas impermeability of graphene.

Small-scale applications, such as graphene coated TEM grids are already available and electron transparent windows for imaging and spectroscopy are being increasingly used. Large-area energy-related applications will require advances in scalable cost-effective 2D-material synthesis and membrane fabrication. Isotope separation for H^+/D^+ is most likely to see rapid development and commercialization due to the potential for substantial reduction in energy consumption compared to existing technologies and these approaches are also likely to be explored for tritium decontamination efforts. Considering processes to commercially produce large-area CVD graphene and h-BN are starting to mature and facile membrane fabrication using hot pressing/lamination and polymer casting have already been demonstrated, these disruptive innovations are likely to be deployed in the nuclear industry in the near future. Incorporation of 2D-materials into proton exchange membranes for flow-batteries, fuel-cells and proton pumps are expected to become viable in the next 5-10 years with scaled-up production offering economies of scale and considering energy saving over the application life-cycle. Further research is needed to inform/guide technological advances towards each of these applications including long-term durability studies under realistic conditions to assess material performance, device integration approaches and membrane manufacturing processes for practical applications.

References and Notes:

1. A. K. Geim, K. S. Novoselov, The rise of graphene. *Nat. Mater.* **6**, 183–191 (2007).
2. A. K. Geim, I. V. Grigorieva, Van der Waals heterostructures. *Nature*. **499**, 419–425 (2013).
3. Y. Peng, Y. Li, Y. Ban, H. Jin, W. Jiao, X. Liu, W. Yang, Metal- organic framework nanosheets as building blocks for molecular sieving membranes. *Science (80-.).* **346**,

1356–1359 (2014).

4. L. Mogg, G.-P. Hao, S. Zhang, C. Bacaksiz, Y.-C. Zou, S. J. Haigh, F. M. Peeters, A. K. Geim, M. Lozada-Hidalgo, Atomically thin micas as proton-conducting membranes. *Nat. Nanotechnol.* **14**, 962–966 (2019).

5. Y. Zhong, B. Cheng, C. Park, A. Ray, S. Brown, F. Mujid, J.-U. U. Lee, H. Zhou, J. Suh, K. H. Lee, A. J. Mannix, K. Kang, S. J. Sibener, D. A. Muller, J. Park, Wafer-scale synthesis of monolayer two-dimensional porphyrin polymers for hybrid superlattices. *Science (80-.).* **9385**, eaax9385 (2019).

6. A. Kolmakov, D. A. Dikin, L. J. Cote, J. Huang, M. K. Abyaneh, M. Amati, L. Gregoratti, S. Günther, M. Kiskinova, Graphene oxide windows for in situ environmental cell photoelectron spectroscopy. *Nat. Nanotechnol.* **6**, 651–657 (2011).

7. L. Wang, M. S. H. Boutilier, P. R. Kidambi, D. Jang, N. G. Hadjiconstantinou, R. Karnik, Fundamental transport mechanisms, fabrication and potential applications of nanoporous atomically thin membranes. *Nat. Nanotechnol.* **12**, 509–522 (2017).

8. L. Prozorovska, P. R. Kidambi, State-of-the-Art and Future Prospects for Atomically Thin Membranes from 2D Materials. *Adv. Mater.* **30**, 1801179 (2018).

9. J. S. Bunch, S. S. Verbridge, J. S. Alden, A. M. van der Zande, J. M. Parpia, H. G. Craighead, P. L. McEuen, Impermeable Atomic Membranes from Graphene Sheets. *Nano Lett.* **8**, 2458–2462 (2008).

10. S. Hu, M. Lozada-Hidalgo, F. C. Wang, A. Mishchenko, F. Schedin, R. R. Nair, E. W. Hill, D. W. Boukhvalov, M. I. Katsnelson, R. A. W. Dryfe, I. V. Grigorieva, H. A. Wu, A. K. Geim, Proton transport through one-atom-thick crystals. *Nature*. **516**, 227–230 (2014).

11. M. Lozada-Hidalgo, S. Hu, O. Marshall, A. Mishchenko, A. N. Grigorenko, R. A. W. W. Dryfe, B. Radha, I. V. Grigorieva, A. K. Geim, Sieving hydrogen isotopes through two-dimensional crystals. *Science (80-.).* **351**, 68–70 (2016).

12. J. Kraus, R. Reichelt, S. Günther, L. Gregoratti, M. Amati, M. Kiskinova, A. Yulaev, I. Vlassiouk, A. Kolmakov, Photoelectron spectroscopy of wet and gaseous samples through graphene membranes. *Nanoscale*. **6**, 14394–14403 (2014).

13. A. A. Balandin, S. Ghosh, W. Bao, I. Calizo, D. Teweldebrhan, F. Miao, C. N. Lau, Superior Thermal Conductivity of Single-Layer Graphene. *Nano Lett.* **8**, 902–907 (2008).

14. C. R. Dean, a F. Young, I. Meric, C. Lee, L. Wang, S. Sorgenfrei, K. Watanabe, T. Taniguchi, P. Kim, K. L. Shepard, J. Hone, Boron nitride substrates for high-quality graphene electronics. *Nat. Nanotechnol.* **5**, 722–726 (2010).

15. K. I. I. Bolotin, K. J. J. Sikes, Z. Jiang, M. Klima, G. Fudenberg, J. Hone, P. Kim, H. L. L. Stormer, Ultrahigh electron mobility in suspended graphene. *Solid State Commun.* **146**, 351–355 (2008).

16. G. Cassabois, P. Valvin, B. Gil, Hexagonal boron nitride is an indirect bandgap semiconductor. *Nat. Photonics*. **10**, 262–266 (2016).

17. Q. Cai, D. Scullion, W. Gan, A. Falin, S. Zhang, K. Watanabe, T. Taniguchi, Y. Chen, E. J. G. Santos, L. H. Li, High thermal conductivity of high-quality monolayer boron nitride

and its thermal expansion. *Sci. Adv.* **5**, eaav0129 (2019).

18. C. Lee, X. Wei, J. W. Kysar, J. Hone, Measurement of the Elastic Properties and Intrinsic Strength of Monolayer Graphene. *Science (80-.).* **321**, 385–388 (2008).

19. A. Falin, Q. Cai, E. J. G. Santos, D. Scullion, D. Qian, R. Zhang, Z. Yang, S. Huang, K. Watanabe, T. Taniguchi, M. R. Barnett, Y. Chen, R. S. Ruoff, L. H. Li, Mechanical properties of atomically thin boron nitride and the role of interlayer interactions. *Nat. Commun.* **8**, 15815 (2017).

20. S. P. Koenig, N. G. Boddeti, M. L. Dunn, J. S. Bunch, Ultrastrong adhesion of graphene membranes. *Nat. Nanotechnol.* **6**, 543–546 (2011).

21. L. Wang, C. M. C. M. Williams, M. S. H. M. S. H. Boutilier, P. R. Kidambi, R. Karnik, Single-Layer Graphene Membranes Withstand Ultrahigh Applied Pressure. *Nano Lett.* **17**, 3081–3088 (2017).

22. R. S. Weatherup, B. Eren, Y. Hao, H. Bluhm, M. B. Salmeron, Graphene Membranes for Atmospheric Pressure Photoelectron Spectroscopy. *J. Phys. Chem. Lett.* **7**, 1622–1627 (2016).

23. D. Cohen-Tanugi, J. C. Grossman, Mechanical Strength of Nanoporous Graphene as a Desalination Membrane. *Nano Lett.* **14**, 6171–6178 (2014).

24. S. P. Koenig, L. Wang, J. Pellegrino, J. S. Bunch, Selective molecular sieving through porous graphene. *Nat. Nanotechnol.* **7**, 728–32 (2012).

25. L. Mogg, S. Zhang, G.-P. Hao, K. Gopinadhan, D. Barry, B. L. Liu, H. M. Cheng, A. K. Geim, M. Lozada-Hidalgo, Perfect proton selectivity in ion transport through two-dimensional crystals. *Nat. Commun.* **10**, 4243 (2019).

26. P. Z. Sun, Q. Yang, W. J. Kuang, Y. V. Stebunov, W. Q. Xiong, J. Yu, R. R. Nair, M. I. Katsnelson, S. J. Yuan, I. V. Grigorieva, M. Lozada-Hidalgo, F. C. Wang, A. K. Geim, Limits on gas impermeability of graphene. *Nature*. **579**, 229–232 (2020).

27. L. Wang, L. W. Drahushuk, L. Cantley, S. P. Koenig, X. Liu, J. Pellegrino, M. S. Strano, J. Scott Bunch, Molecular valves for controlling gas phase transport made from discrete ångström-sized pores in graphene. *Nat. Nanotechnol.* **10**, 785–790 (2015).

28. L. Tsetseris, S. T. Pantelides, Graphene: An impermeable or selectively permeable membrane for atomic species? *Carbon N. Y.* **67**, 58–63 (2014).

29. M. Miao, M. B. Nardelli, Q. Wang, Y. Liu, First principles study of the permeability of graphene to hydrogen atoms. *Phys. Chem. Chem. Phys.* **15**, 16132 (2013).

30. O. Leenaerts, B. Partoens, F. M. Peeters, Graphene: A perfect nanoballoon. *Appl. Phys. Lett.* **93**, 193107 (2008).

31. M. Seel, R. Pandey, Proton and hydrogen transport through two-dimensional monolayers. *2D Mater.* **3**, 025004 (2016).

32. L. W. Drahushuk, L. Wang, S. P. Koenig, J. S. Bunch, M. S. Strano, Analysis of time-varying, stochastic gas transport through graphene membranes. *ACS Nano*. **10**, 786–795 (2016).

33. O. Lehtinen, J. Kotakoski, A. V. Krasheninnikov, A. Tolvanen, K. Nordlund, J. Keinonen,

Effects of ion bombardment on a two-dimensional target: Atomistic simulations of graphene irradiation. *Phys. Rev. B*. **81**, 153401 (2010).

34. K. Yoon, A. Rahnamoun, J. L. Swett, V. Iberi, D. A. Cullen, I. V. Vlassiouk, A. Belianinov, S. Jesse, X. Sang, O. S. Ovchinnikova, A. J. Rondinone, R. R. Unocic, A. C. T. Van Duin, Atomistic-Scale Simulations of Defect Formation in Graphene under Noble Gas Ion Irradiation. *ACS Nano*. **10**, 8376–8384 (2016).

35. K. Alexandrou, Ionizing Radiation Effects on Graphene Based Field Effects Transistors. *ProQuest Diss. Theses*, 148 (2016).

36. A. V. Krasheninnikov, Are two-dimensional materials radiation tolerant? *Nanoscale Horizons*. **5**, 1447–1452 (2020).

37. T. Susi, J. C. Meyer, J. Kotakoski, Quantifying transmission electron microscopy irradiation effects using two-dimensional materials. *Nat. Rev. Phys.* **1**, 397–405 (2019).

38. E. Cobas, A. L. Friedman, O. M. J. Van'T Erve, J. T. Robinson, B. T. Jonker, Graphene as a tunnel barrier: Graphene-based magnetic tunnel junctions. *Nano Lett.* **12**, 3000–3004 (2012).

39. X. Zhu, S. Lei, S.-H. S.-P. S. H. S. P. Tsai, X. Zhang, J. Liu, G. Yin, M. Tang, C. M. Torres, A. Navabi, Z. Jin, S.-H. S.-P. S. H. S. P. Tsai, H. Qasem, Y. Wang, R. Vajtai, R. K. Lake, P. M. Ajayan, K. L. Wang, A Study of Vertical Transport through Graphene toward Control of Quantum Tunneling. *Nano Lett.* **18**, 682–688 (2018).

40. J. Xue, J. Sanchez-Yamagishi, D. Bulmash, P. Jacquod, A. Deshpande, K. Watanabe, T. Taniguchi, P. Jarillo-Herrero, B. J. Leroy, Scanning tunnelling microscopy and spectroscopy of ultra-flat graphene on hexagonal boron nitride. *Nat. Mater.* **10**, 282–285 (2011).

41. G. H. Lee, Y. J. Yu, C. Lee, C. Dean, K. L. Shepard, P. Kim, J. Hone, Electron tunneling through atomically flat and ultrathin hexagonal boron nitride. *Appl. Phys. Lett.* **99**, 243114 (2011).

42. L. Britnell, R. V. Gorbachev, R. Jalil, B. D. Belle, F. Schedin, M. I. Katsnelson, L. Eaves, S. V. Morozov, A. S. Mayorov, N. M. R. Peres, A. H. Castro Neto, J. Leist, A. K. Geim, L. A. Ponomarenko, K. S. Novoselov, Electron Tunneling through Ultrathin Boron Nitride Crystalline Barriers. *Nano Lett.* **12**, 1707–1710 (2012).

43. E. C. Ahn, 2D materials for spintronic devices. *npj 2D Mater. Appl.* **4**, 17 (2020).

44. F. Giannazzo, G. Greco, F. Roccaforte, S. Sonde, Vertical Transistors Based on 2D Materials: Status and Prospects. *Crystals*. **8**, 70 (2018).

45. J. A. Yan, J. A. Driscoll, B. K. Wyatt, K. Varga, S. T. Pantelides, Time-domain simulation of electron diffraction in crystals. *Phys. Rev. B - Condens. Matter Mater. Phys.* **84**, 224117 (2011).

46. J.-N. N. Longchamp, T. Latychevskaia, C. Escher, H.-W. W. Fink, Low-energy electron transmission imaging of clusters on free-standing graphene. *Appl. Phys. Lett.* **101**, 113117 (2012).

47. J. Y. Mutus, L. Livadaru, J. T. Robinson, R. Urban, M. H. Salomons, M. Cloutier, R. A.

Wolkow, Low-energy electron point projection microscopy of suspended graphene, the ultimate "microscope slide." *New J. Phys.* **13**, 063011 (2011).

48. G. Hassink, R. Wanke, I. Rastegar, W. Braun, C. Stephanos, P. Herlinger, J. H. Smet, J. Mannhart, Transparency of graphene for low-energy electrons measured in a vacuum-triode setup. *APL Mater.* **3**, 076106 (2015).

49. R. S. Weatherup, 2D Material Membranes for Operando Atmospheric Pressure Photoelectron Spectroscopy. *Top. Catal.* **61**, 2085–2102 (2018).

50. S. Tanuma, C. J. Powell, D. R. Penn, Calculations of electron inelastic mean free paths. IX. Data for 41 elemental solids over the 50 eV to 30 keV range. *Surf. Interface Anal.* **43**, 689–713 (2011).

51. M. Xu, D. Fujita, J. Gao, N. Hanagata, Auger electron spectroscopy: A rational method for determining thickness of graphene films. *ACS Nano*. **4**, 2937–2945 (2010).

52. J. C. Meyer, F. Eder, S. Kurasch, V. Skakalova, J. Kotakoski, H. J. Park, S. Roth, A. Chuvilin, S. Eyhusen, G. Benner, A. V. Krasheninnikov, U. Kaiser, Accurate measurement of electron beam induced displacement cross sections for single-layer graphene. *Phys. Rev. Lett.* **108**, 1–6 (2012).

53. J. C. Meyer, A. Chuvilin, G. Algara-Siller, J. Biskupek, U. Kaiser, Selective sputtering and atomic resolution imaging of atomically thin boron nitride membranes. *Nano Lett.* **9**, 2683–2689 (2009).

54. S. M. Gilbert, G. Dunn, A. Azizi, T. Pham, B. Shevitski, E. Dimitrov, S. Liu, S. Aloni, A. Zettl, Fabrication of Subnanometer-Precision Nanopores in Hexagonal Boron Nitride. *Sci. Rep.* **7**, 15096 (2017).

55. C. Thiele, A. Felten, T. J. Echtermeyer, A. C. Ferrari, C. Casiraghi, H. V. Löhneysen, R. Krupke, Electron-beam-induced direct etching of graphene. *Carbon N. Y.* **64**, 84–91 (2013).

56. C. Elbadawi, T. T. Tran, M. Kolíbal, T. Šikola, J. Scott, Q. Cai, L. H. Li, T. Taniguchi, K. Watanabe, M. Toth, I. Aharonovich, C. Lobo, Electron beam directed etching of hexagonal boron nitride. *Nanoscale*. **8**, 16182–16186 (2016).

57. S. Sinha, J. H. Warner, Recent Progress in Using Graphene as an Ultrathin Transparent Support for Transmission Electron Microscopy. *Small Struct.*, 2000049 (2021).

58. M. I. Walker, P. Braeuninger-Weimer, R. S. Weatherup, S. Hofmann, U. F. Keyser, Measuring the proton selectivity of graphene membranes. *Appl. Phys. Lett.* **107**, 213104 (2015).

59. J. L. Achtyl, R. R. Unocic, L. Xu, Y. Cai, M. Raju, W. Zhang, R. L. Sacci, I. V. Vlassiouk, P. F. Fulvio, P. Ganesh, D. J. Wesolowski, S. Dai, A. C. T. van Duin, M. Neurock, F. M. Geiger, Aqueous proton transfer across single-layer graphene. *Nat. Commun.* **6**, 6539 (2015).

60. M. Lozada-Hidalgo, S. Zhang, S. Hu, V. G. Kravets, F. J. Rodriguez, A. Berdyugin, A. Grigorenko, A. K. Geim, Giant photoeffect in proton transport through graphene membranes. *Nat. Nanotechnol.* **13**, 300–303 (2018).

61. I. Poltavsky, L. Zheng, M. Mortazavi, A. Tkatchenko, Quantum tunneling of thermal protons through pristine graphene. *J. Chem. Phys.* **148**, 204707 (2018).

62. Y. Feng, J. Chen, W. Fang, E. G. Wang, A. Michaelides, X. Z. Li, Hydrogenation Facilitates Proton Transfer through Two-Dimensional Honeycomb Crystals. *J. Phys. Chem. Lett.* **8**, 6009–6014 (2017).

63. J. M. H. Kroes, A. Fasolino, M. I. Katsnelson, Density functional based simulations of proton permeation of graphene and hexagonal boron nitride. *Phys. Chem. Chem. Phys.* **19**, 5813–5817 (2017).

64. M. Bartolomei, M. I. Hernández, J. Campos-Martínez, R. Hernández-Lamoneda, Graphene multi-protonation: A cooperative mechanism for proton permeation. *Carbon N. Y.* **144**, 724–730 (2019).

65. Q. Zhang, M. Ju, L. Chen, X. C. Zeng, Differential Permeability of Proton Isotopes through Graphene and Graphene Analogue Monolayer. *J. Phys. Chem. Lett.* **7**, 3395–3400 (2016).

66. S. Bukola, Y. Liang, C. Korzeniewski, J. Harris, S. Creager, Selective Proton/Deuteron Transport through Nafion|Graphene|Nafion Sandwich Structures at High Current Density. *J. Am. Chem. Soc.* **140**, 1743–1752 (2018).

67. M. Lozada-Hidalgo, S. Zhang, S. Hu, A. Esfandiar, I. V Grigorieva, A. K. Geim, Scalable and efficient separation of hydrogen isotopes using graphene-based electrochemical pumping. *Nat. Commun.* **8**, 15215 (2017).

68. Y. An, A. F. Oliveira, T. Brumme, A. Kuc, T. Heine, Stone–Wales Defects Cause High Proton Permeability and Isotope Selectivity of Single-Layer Graphene. *Adv. Mater.* **32**, 2002442 (2020).

69. P. Y. Huang, C. S. Ruiz-Vargas, A. M. van der Zande, W. S. Whitney, M. P. Levendorf, J. W. Kevek, S. Garg, J. S. Alden, C. J. Hustedt, Y. Zhu, J. Park, P. L. McEuen, D. a Muller, Grains and grain boundaries in single-layer graphene atomic patchwork quilts. *Nature*. **469**, 389–92 (2011).

70. E. Griffin, L. Mogg, G. P. Hao, G. P. Hao, G. Kalon, G. Kalon, C. Bacaksiz, G. Lopez-Polin, G. Lopez-Polin, T. Y. Zhou, V. Guarochico, J. Cai, C. Neumann, A. Winter, M. Mohn, J. H. Lee, J. Lin, J. Lin, U. Kaiser, I. V. Grigorieva, K. Suenaga, B. Özyilmaz, H. M. Cheng, H. M. Cheng, W. Ren, A. Turchanin, F. M. Peeters, A. K. Geim, M. Lozada-Hidalgo, Proton and Li-Ion Permeation through Graphene with Eight-Atom-Ring Defects. *ACS Nano*. **14**, 7280–7286 (2020).

71. S. Bukola, S. E. Creager, A charge-transfer resistance model and Arrhenius activation analysis for hydrogen ion transmission across single-layer graphene. *Electrochim. Acta*. **296**, 1–7 (2019).

72. M. I. Walker, R. S. Weatherup, N. A. W. Bell, S. Hofmann, U. F. Keyser, Free-standing graphene membranes on glass nanopores for ionic current measurements. *Appl. Phys. Lett.* **106**, 023119 (2015).

73. M. I. Walker, K. Ubych, V. Saraswat, E. A. Chalklen, P. Braeuninger-Weimer, S. Caneva, R. S. Weatherup, S. Hofmann, U. F. Keyser, Extrinsic Cation Selectivity of 2D

Membranes. *ACS Nano*. **11**, 1340–1346 (2017).

74. P. Chaturvedi, I. V. Vlassiouk, D. A. Cullen, A. J. Rondinone, N. V. Lavrik, S. N. Smirnov, Ionic conductance through graphene: Assessing its applicability as a proton selective membrane. *ACS Nano*. **13**, 12109–12119 (2019).

75. Z. Zeng, R. Song, S. Zhang, X. Han, Z. Zhu, X. Chen, L. Wang, *Nano Lett.*, in press, doi:10.1021/acs.nanolett.1c00813.

76. Y. Hernandez, V. Nicolosi, M. Lotya, F. M. Blighe, Z. Sun, S. De, I. T. Mcgovern, B. Holland, M. Byrne, Y. Gun 'ko, J. Boland, P. Niraj, G. Duesberg, S. Krishnamurthy, R. Goodhue, J. Hutchison, V. Scardaci, A. C. Ferrari, J. N. Coleman, Y. Gunko, J. Boland, P. Niraj, G. Duesberg, S. Krishnamurti, R. Goodhue, J. Hutchison, V. Scardaci, A. C. Ferrari, J. N. Coleman, High yield production of graphene by liquid phase exfoliation of graphite. *Nat. Nanotechnol.* **3**, 563–8 (2008).

77. X. Li, W. Cai, J. An, S. Kim, J. Nah, D. Yang, R. D. Piner, A. Velamakanni, I. Jung, E. Tutuc, S. K. Banerjee, L. Colombo, R. S. Ruoff, Large-area synthesis of high quality and uniform graphene films on copper foils. *Science (80-.).* **324**, 1312–1314 (2009).

78. K. K. Kim, A. Hsu, X. Jia, S. M. Kim, Y. Shi, M. Hofmann, D. Nezich, J. F. Rodriguez-Nieva, M. Dresselhaus, T. Palacios, J. Kong, Synthesis of monolayer hexagonal boron nitride on Cu foil using chemical vapor deposition. *Nano Lett.* **12**, 161–6 (2012).

79. T. Zhao, C. Xu, W. Ma, Z. Liu, T. Zhou, Z. Liu, S. Feng, M. Zhu, N. Kang, D.-M. Sun, H.-M. Cheng, W. Ren, Ultrafast growth of nanocrystalline graphene films by quenching and grain-size-dependent strength and bandgap opening. *Nat. Commun.* **10**, 4854 (2019).

80. C. T. Toh, H. Zhang, J. Lin, A. S. Mayorov, Y. P. Wang, C. M. Orofeo, D. B. Ferry, H. Andersen, N. Kakenov, Z. Guo, I. H. Abidi, H. Sims, K. Suenaga, S. T. Pantelides, B. Özyilmaz, Synthesis and properties of free-standing monolayer amorphous carbon. *Nature*. **577**, 199–203 (2020).

81. Z. Cai, B. Liu, X. Zou, H. M. Cheng, Chemical Vapor Deposition Growth and Applications of Two-Dimensional Materials and Their Heterostructures. *Chem. Rev.* **118** (2018), pp. 6091–6133.

82. P. R. Kidambi, D. D. Mariappan, N. T. Dee, A. Vyatskikh, S. Zhang, R. Karnik, A. J. Hart, A Scalable Route to Nanoporous Large-Area Atomically Thin Graphene Membranes by Roll-to-Roll Chemical Vapor Deposition and Polymer Support Casting. *ACS Appl. Mater. Interfaces*. **10**, 10369–10378 (2018).

83. L. Wang, X. Xu, L. Zhang, R. Qiao, M. Wu, Z. Wang, S. Zhang, J. Liang, Z. Zhang, Z. Zhang, W. Chen, X. Xie, J. Zong, Y. Shan, Y. Guo, M. Willinger, H. Wu, Q. Li, W. Wang, P. Gao, S. Wu, Y. Zhang, Y. Jiang, D. Yu, E. Wang, X. Bai, Z.-J. Wang, F. Ding, K. Liu, Epitaxial growth of a 100-square-centimetre single-crystal hexagonal boron nitride monolayer on copper. *Nature*. **570**, 91–95 (2019).

84. T. Kobayashi, M. Bando, N. Kimura, K. Shimizu, K. Kadono, N. Umezu, K. Miyahara, S. Hayazaki, S. Nagai, Y. Mizuguchi, Y. Murakami, D. Hobara, Production of a 100-m-long high-quality graphene transparent conductive film by roll-to-roll chemical vapor deposition and transfer process. *Appl. Phys. Lett.* **102**, 023112 (2013).

85. S. C. O'Hern, C. A. Stewart, M. S. H. H. Boutilier, J. C. Idrobo, S. Bhaviripudi, S. K. Das, J. Kong, T. Laoui, M. Atieh, R. Karnik, S. C. O'Hern, C. A. Stewart, M. S. H. H. Boutilier, J. C. Idrobo, S. Bhaviripudi, S. K. Das, J. Kong, T. Laoui, M. Atieh, R. Karnik, Selective Molecular Transport through Intrinsic Defects in a Single Layer of CVD Graphene. *ACS Nano*. **6**, 10130–10138 (2012).

86. N. Petrone, C. R. Dean, I. Meric, A. M. Van Der Zande, P. Y. Huang, L. Wang, D. Muller, K. L. Shepard, J. Hone, Chemical vapor deposition-derived graphene with electrical performance of exfoliated graphene. *Nano Lett.* **12**, 2751–2756 (2012).

87. X. Xu, Z. Zhang, J. Dong, D. Yi, J. Niu, M. Wu, L. Lin, R. Yin, M. Li, J. Zhou, S. Wang, J. Sun, X. Duan, P. Gao, Y. Jiang, X. Wu, H. Peng, R. S. Ruoff, Z. Liu, D. Yu, E. Wang, F. Ding, K. Liu, Ultrafast epitaxial growth of metre-sized single-crystal graphene on industrial Cu foil. *Sci. Bull.* **62**, 1074–1080 (2017).

88. J. H. Lee, E. K. Lee, W. J. Joo, Y. Jang, B. S. Kim, J. Y. Lim, S. H. Choi, S. J. Ahn, J. R. Ahn, M. H. Park, C. W. Yang, B. L. Choi, S. W. Hwang, D. Whang, Wafer-scale growth of single-crystal monolayer graphene on reusable hydrogen-terminated germanium. *Science (80-.).* **344**, 286–289 (2014).

89. J. S. Lee, S. H. Choi, S. J. Yun, Y. I. Kim, S. Boandoh, J. H. Park, B. G. Shin, H. Ko, S. H. Lee, Y. M. Kim, Y. H. Lee, K. K. Kim, S. M. Kim, Wafer-scale single-crystal hexagonal boron nitride film via self-collimated grain formation. *Science (80-.).* **362**, 817–821 (2018).

90. T. Wu, X. Zhang, Q. Yuan, J. Xue, G. Lu, Z. Liu, H. Wang, H. Wang, F. Ding, Q. Yu, X. Xie, M. Jiang, Fast growth of inch-sized single-crystalline graphene from a controlled single nucleus on Cu–Ni alloys. *Nat. Mater.* **15**, 43–47 (2015).

91. X. Xu, Z. Zhang, L. Qiu, J. Zhuang, L. Zhang, H. Wang, C. Liao, H. Song, R. Qiao, P. Gao, Z. Hu, L. Liao, Z. Liao, D. Yu, E. Wang, F. Ding, H. Peng, K. Liu, Ultrafast growth of single-crystal graphene assisted by a continuous oxygen supply. *Nat. Nanotechnol.* **11**, 1–13 (2016).

92. I. V. Vlassiouk, Y. Stehle, P. R. Pudasaini, R. R. Unocic, P. D. Rack, A. P. Baddorf, I. N. Ivanov, N. V. Lavrik, F. List, N. Gupta, K. V. Bets, B. I. Yakobson, S. N. Smirnov, Evolutionary selection growth of two-dimensional materials on polycrystalline substrates. *Nat. Mater.* **17**, 318–322 (2018).

93. P. R. Kidambi, M. S. H. M. S. H. Boutilier, L. Wang, D. Jang, J. Kim, R. Karnik, Selective Nanoscale Mass Transport across Atomically Thin Single Crystalline Graphene Membranes. *Adv. Mater.* **29**, 1605896 (2017).

94. P. R. Kidambi, R. A. Terry, L. Wang, M. S. H. Boutilier, D. Jang, J. Kong, R. Karnik, Assessment and control of the impermeability of graphene for atomically thin membranes and barriers. *Nanoscale*. **9**, 8496–8507 (2017).

95. S. C. O'Hern, D. Jang, S. Bose, J. C. Idrobo, Y. Song, T. Laoui, J. Kong, R. Karnik, Nanofiltration across defect-sealed nanoporous monolayer graphene. *Nano Lett.* **15**, 3254–3260 (2015).

96. P. Cheng, M. M. Kelly, N. K. Moehring, W. Ko, A. P. Li, J. C. Idrobo, M. S. H. Boutilier, P. R. Kidambi, Facile Size-Selective Defect Sealing in Large-Area Atomically Thin

Graphene Membranes for Sub-Nanometer Scale Separations. *Nano Lett.* **20**, 5951–5959 (2020).

97. J. M. Yuk, J. Park, P. Ercius, K. Kim, D. J. Hellebusch, M. F. Crommie, J. Y. Lee, A. Zettl, A. P. Alivisatos, High-Resolution EM of Colloidal Nanocrystal Growth Using Graphene Liquid Cells. *Science (80-.).* **336**, 61–64 (2012).

98. P. R. Kidambi, G. D. Nguyen, S. Zhang, Q. Chen, J. Kong, J. Warner, A.-P. Li, R. Karnik, Facile Fabrication of Large-Area Atomically Thin Membranes by Direct Synthesis of Graphene with Nanoscale Porosity. *Adv. Mater.* **1804977**, 1804977 (2018).

99. P. Cheng, N. K. Moehring, J. C. Idrobo, I. N. Ivanov, P. R. Kidambi, Scalable synthesis of nanoporous atomically thin graphene membranes for dialysis and molecular separations via facile isopropanol-assisted hot lamination. *Nanoscale*. **13**, 2825–2837 (2021).

100. Y. Wang, Y. Zheng, X. Xu, E. Dubuisson, Q. Bao, J. Lu, K. P. Loh, Electrochemical delamination of CVD-grown graphene film: Toward the recyclable use of copper catalyst. *ACS Nano*. **5**, 9927–9933 (2011).

101. The Price Of Graphene – Graphenea, (available at https://www.graphenea.com/pages/graphene-price#.X-uoxdhKhPY).

102. A. Zurutuza, C. Marinelli, Challenges and opportunities in graphene commercialization. *Nat. Nanotechnol.* **9**, 730–734 (2014).

103. S. Satyapal, U. Department of Energy Hydrogen, F. C. Program, "DOE Hydrogen and Fuel Cell Perspectives and Overview of the International Partnership for Hydrogen and Fuel Cells in the Economy (IPHE)" (2020), (available at https://www.energy.gov/sites/prod/files/2020/07/f77/hfto-satyapal-gabi-workshop-jul20.pdf).

104. G. Alberti, M. Casciola, L. Massinelli, B. Bauer, Polymeric proton conducting membranes for medium temperature fuel cells (110-160°C). *J. Memb. Sci.* **185**, 73–81 (2001).

105. K. A. Mauritz, R. B. Moore, State of understanding of Nafion. *Chem. Rev.* **104**, 4535–4585 (2004).

106. C. E. Thomas, Fuel cell and battery electric vehicles compared. *Int. J. Hydrogen Energy*. **34**, 6005–6020 (2009).

107. Y. Wang, D. F. Ruiz Diaz, K. S. Chen, Z. Wang, X. C. Adroher, Materials, technological status, and fundamentals of PEM fuel cells – A review. *Mater. Today*. **32**, 178–203 (2020).

108. M. B. Karimi, F. Mohammadi, K. Hooshyari, Recent approaches to improve Nafion performance for fuel cell applications: A review. *Int. J. Hydrogen Energy*. **44**, 28919–28938 (2019).

109. S. I. Yoon, D. J. Seo, G. Kim, M. Kim, C. Y. Jung, Y. G. Yoon, S. H. Joo, T. Y. Kim, H. S. Shin, AA′-Stacked Trilayer Hexagonal Boron Nitride Membrane for Proton Exchange Membrane Fuel Cells. *ACS Nano*. **12**, 10764–10771 (2018).

110. S. M. Holmes, P. Balakrishnan, V. S. Kalangi, X. Zhang, M. Lozada-Hidalgo, P. M. Ajayan, R. R. Nair, 2D Crystals Significantly Enhance the Performance of a Working Fuel

Cell. *Adv. Energy Mater.* **7**, 1–7 (2017).

111. X. H. H. Yan, R. Wu, J. B. B. Xu, Z. Luo, T. S. S. Zhao, A monolayer graphene – Nafion sandwich membrane for direct methanol fuel cells. *J. Power Sources*. **311**, 188–194 (2016).

112. M. S. H. Boutilier, D. Jang, J.-C. Idrobo, P. R. Kidambi, N. G. Hadjiconstantinou, R. Karnik, Molecular Sieving Across Centimeter-Scale Single-Layer Nanoporous Graphene Membranes. *ACS Nano*. **11**, 5726–5736 (2017).

113. L. H. Li, J. Cervenka, K. Watanabe, T. Taniguchi, Y. Chen, Strong oxidation resistance of atomically thin boron nitride nanosheets. *ACS Nano*. **8**, 1457–1462 (2014).

114. Z. P. Cano, D. Banham, S. Ye, A. Hintennach, J. Lu, M. Fowler, Z. Chen, Batteries and fuel cells for emerging electric vehicle markets. *Nat. Energy*. **3**, 279–289 (2018).

115. B. D. James, J. A. Kalinoski, K. N. Baum, *Mass Production Cost Estimation for Direct H 2 PEM Fuel Cell Systems for Automotive Applications : 2009 Update, US department of energy report* (2010; https://www.energy.gov/sites/prod/files/2017/06/f34/fcto_sa_2016_pemfc_transportation_cost_analysis.pdf).

116. Fuel Cells | Department of Energy, (available at https://www.energy.gov/eere/fuelcells/fuel-cells).

117. G. Saur, A. Milbrandt, Renewable Hydrogen Potential from Biogas in the United States. *Natl. Renew. Energy Lab.*, 1–44 (2014).

118. G. L. Soloveichik, Flow Batteries: Current Status and Trends. *Chem. Rev.* **115**, 11533–11558 (2015).

119. UniEnergy Technologies - Rongke Power | EcoPartnerships, (available at https://ecopartnerships.lbl.gov/partnership/unienergy).

120. J. Liu, L. Yu, X. Cai, U. Khan, Z. Cai, J. Xi, B. Liu, F. Kang, Sandwiching h-BN monolayer films between sulfonated poly(ether ether ketone) and nafion for proton exchange membranes with improved ion selectivity. *ACS Nano*. **13**, 2094–2102 (2019).

121. S. Bukola, Z. Li, J. Zack, C. Antunes, C. Korzeniewski, G. Teeter, J. Blackburn, B. Pivovar, Single-layer graphene as a highly selective barrier for vanadium crossover with high proton selectivity. *J. Energy Chem.* **59**, 419–430 (2021).

122. Q. Chen, Y.-Y. Du, K.-M. Li, H.-F. Xiao, W. Wang, W.-M. Zhang, Graphene enhances the proton selectivity of porous membrane in vanadium flow batteries. *Mater. Des.* **113**, 149–156 (2017).

123. A. I. Miller, "Heavy Water: A Manufacturers' Guide for the Hydrogen Century" (2001).

124. H. K. Rae, *Selecting Heavy Water Processes* (1978).

125. S. Tosti, A. Pozio, Membrane Processes for the Nuclear Fusion Fuel Cycle. *Membranes (Basel).* **8**, 96 (2018).

126. "Report for the Second of Two 2008 Charges to the Nuclear Science Advisory Committee on the Isotope Development and Production for Research and Applications Program Isotopes for the Nation's Future A Long Range Plan NSAC Isotopes Subcommittee"

(2009), (available at https://science.osti.gov/-/media/np/nsac/pdf/docs/nsaci_ii_report.pdf).

127. C. Wang, Q. Qiao, T. Shokuhfar, R. F. Klie, High-Resolution Electron Microscopy and Spectroscopy of Ferritin in Biocompatible Graphene Liquid Cells and Graphene Sandwiches. *Adv. Mater.* **26**, 3410–3414 (2014).

128. A. Yulaev, H. Guo, E. Strelcov, L. Chen, I. Vlassiouk, A. Kolmakov, Graphene Microcapsule Arrays for Combinatorial Electron Microscopy and Spectroscopy in Liquids. *ACS Appl. Mater. Interfaces*. **9**, 26492–26502 (2017).

129. J. Park, K. Koo, N. Noh, J. H. Chang, J. Y. Cheong, K. S. Dae, J. S. Park, S. Ji, I.-D. Kim, J. M. Yuk, Graphene Liquid Cell Electron Microscopy: Progress, Applications, and Perspectives. *ACS Nano*. **15**, 288–308 (2021).

130. F. M. Ross, Opportunities and challenges in liquid cell electron microscopy. *Science (80-.).* **350**, aaa9886–aaa9886 (2015).

131. Y. Han, K. X. Nguyen, Y. Ogawa, J. Park, D. A. Muller, Atomically Thin Graphene Windows That Enable High Contrast Electron Microscopy without a Specimen Vacuum Chamber. *Nano Lett.* **16**, 7427–7432 (2016).

132. J. C. Meyer, C. O. Girit, M. F. Crommie, A. Zettl, Imaging and dynamics of light atoms and molecules on graphene. *Nature*. **454**, 319–322 (2008).

133. R. R. Nair, P. Blake, J. R. Blake, R. Zan, S. Anissimova, U. Bangert, A. P. Golovanov, S. V. Morozov, A. K. Geim, K. S. Novoselov, T. Latychevskaia, Graphene as a transparent conductive support for studying biological molecules by transmission electron microscopy. *Appl. Phys. Lett.* **97**, 153102 (2010).

134. K. Naydenova, M. J. Peet, C. J. Russo, Multifunctional graphene supports for electron cryomicroscopy. *Proc. Natl. Acad. Sci. U. S. A.* **116**, 11718–11724 (2019).

135. Y. Han, X. Fan, H. Wang, F. Zhao, C. G. Tully, J. Kong, N. Yao, N. Yan, High-yield monolayer graphene grids for near-atomic resolution cryoelectron microscopy. *Proc. Natl. Acad. Sci. U. S. A.* **117**, 1009–1014 (2020).

136. J. D. Stoll, A. Kolmakov, Electron transparent graphene windows for environmental scanning electron microscopy in liquids and dense gases. *Nanotechnology*. **23**, 505704 (2012).

137. S. Nemšák, E. Strelcov, T. Duchoň, H. Guo, J. Hackl, A. Yulaev, I. Vlassiouk, D. N. Mueller, C. M. Schneider, A. Kolmakov, Interfacial Electrochemistry in Liquids Probed with Photoemission Electron Microscopy. *J. Am. Chem. Soc.* **139**, 18138–18141 (2017).

138. K. Koo, K. S. Dae, Y. K. Hahn, J. M. Yuk, Live Cell Electron Microscopy Using Graphene Veils. *Nano Lett.* **20**, 4708–4713 (2020).

139. S. Bukola, K. Beard, C. Korzeniewski, J. M. Harris, S. E. Creager, Single-Layer Graphene Sandwiched between Proton-Exchange Membranes for Selective Proton Transmission. *ACS Appl. Nano Mater.* **2**, 964–974 (2019).

140. B. Jiang, L. Wu, L. Yu, X. Qiu, J. Xi, A comparative study of Nafion series membranes for vanadium redox flow batteries. *J. Memb. Sci.* **510**, 18–26 (2016).

141. S. Slade, S. A. Campbell, T. R. Ralph, F. C. Walsh, Ionic Conductivity of an Extruded

Nafion 1100 EW Series of Membranes. *J. Electrochem. Soc.* **149**, A1556 (2002).

142. N. T. Ekanayake, J. Huang, J. Jakowski, B. G. Sumpter, S. Garashchuk. Relevance of the Nuclear Quantum Effects on the Proton/Deuteron Transmission through Hexagonal Boron Nitride and Graphene Monolayers. *J. Phys. Chem. C.* **121**, 24335–24344 (2017).

143. L. Shi, A. X, G. Chen, T. Zhao. Theoretical Understanding of Mechanisms of Proton Exchange Membranes Made of 2D Crystals with Ultrahigh Selectivity. *J. Phys. Chem. Lett.* **8**, 4354–4361 (2017).

144. W. L. Wang, E. Kaxiras. Graphene Hydrate: Theoretical Prediction of a New Insulating Form of Graphene *New J. Phys.* **12**, 125012 (2010).

145. T. Hao, Y. Xu, T. Hao. Conductivity Equations of Protons Transporting through 2D Crystals Obtained with the Rate Process Theory and Free Volume Concept. *Chem. Phys. Lett.* **698**, 67-71 (2018).

Acknowledgments: Authors acknowledge helpful input from Dr. Andrei Kolmakov, Prof. Ronald Schrimpf, and stimulating discussions with Prof. Sokrates Pantelides, Prof. Stephen Creager, Prof. Rohit Karnik, Prof. Peter N. Pintauro, Prof. John A. Hart, Prof. Christina Payne, Dr. Ethan Balkin, and Dr. Daniel Matuszak.

Funding: P.R.K. acknowledges funding from NSF CAREER award #1944134 and 2020-2021 ECS-Toyota Young Investigator Fellowship.

Author contributions: P.R.K. wrote the paper with input from P.C. and N.K.M. N.K.M and P.C. made the figures, contributed to discussions and writing. P.C. and N.K.M contributed equally.

Competing interests: P.R.K. acknowledges stake in a company aimed at commercializing 2D-materials with patents awarded/pending.

Data and materials availability: References to all data are provided in the manuscript.

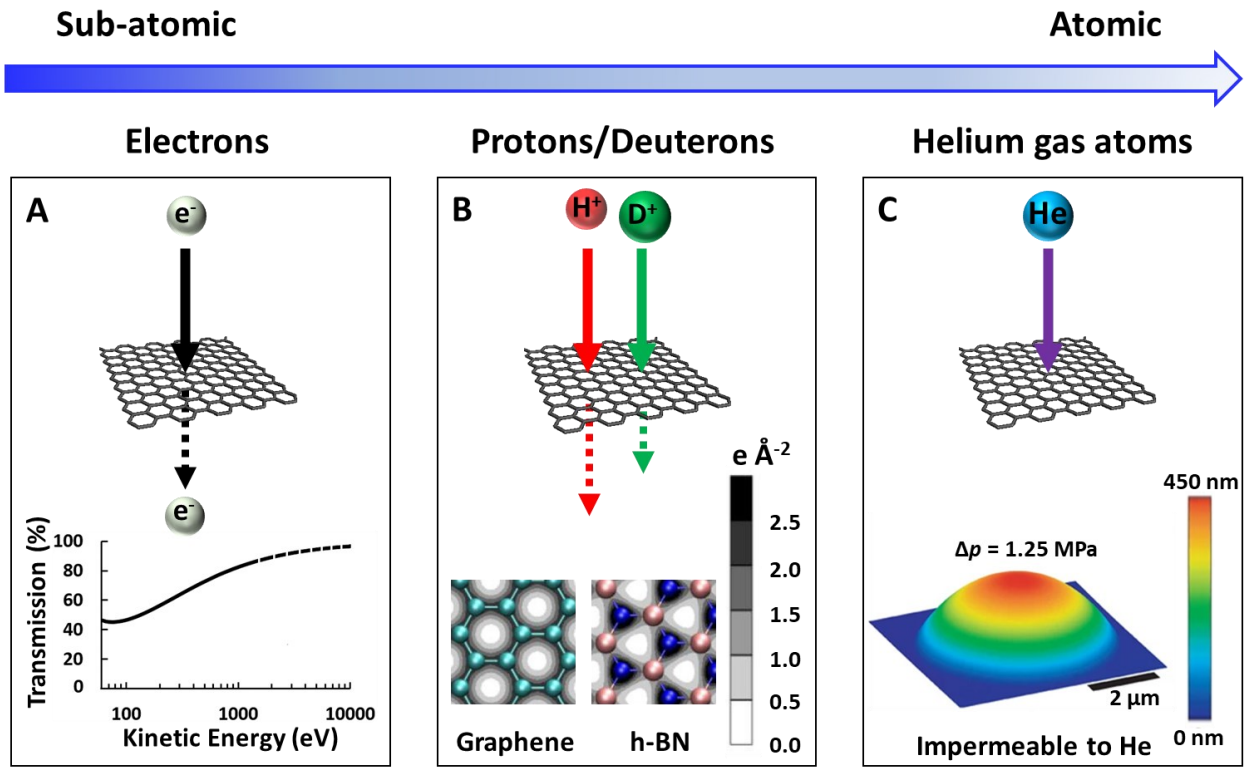

Figure 1. Transport through the atomically thin lattice of graphene and h-BN.

A) Electrons tunnel through the lattice of monolayer graphene and h-BN. The transmission of energetic electrons, however, depends on their kinetic energy. Solid line up to ~1600eV indicates regions where measured values are available in literature. (Re-drawn using data in Ref (*12*, *49*).) B) Electric-field-driven thermal protons and deuterons transport through the graphene and h-BN lattice due to pores in the electron cloud. Inset shows integrated charge density (electrons/Å^2) for graphene and h-BN. (Adapted with permission from Ref (*10*).) C) The graphene lattice is impermeable to helium atoms and other gases. Inset shows a 3-D rendering of an AFM image of the graphene sealing gas molecules under a pressure difference of 1.25 MPa. (Adapted with permission from Ref(*20*).)

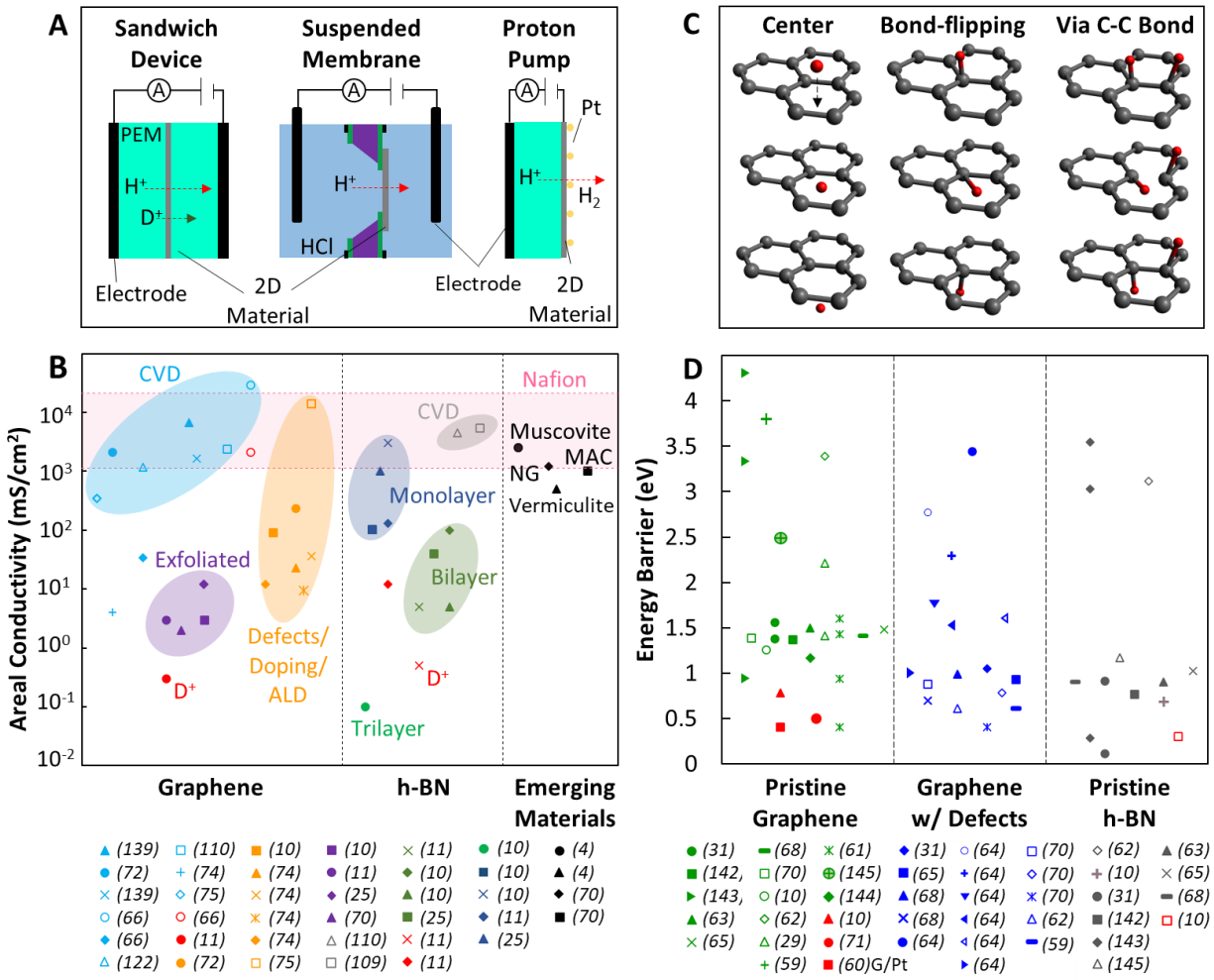

Figure 2. Experimental and theoretical aspects of proton permeation through 2D-materials.

A) Schematics of experimental device configurations used to measure proton transport.(*10*, *60*) Nafion-2D-material-Nafion sandwich devices (left), suspended 2D-material membranes separating liquid electrolytes (middle), Nafion-2D-material-Pt proton pump devices (right). B) Experimentally measured areal proton conductivity values for graphene, h-BN, other emerging materials and the industry standard ionomer Nafion reported in literature. Red symbols represent deuteron areal conductivities. Most of the reported conductivity values in the literature are measured with 0.1M HCl electrolyte or H_2 gas/methanol feed to the devices/fuel-cells except Ref.(*25*), Ref.(*75*) with 1M HCl and Ref.(*122*) with 0.5M H_2SO_4 in vanadium flow batteries. Values for Nafion are extracted from Ref. (*66*, *139–141*). Different symbols with the same reference represent distinct material structure/defects. C) Schematics of mechanisms of proton transport through graphene proposed by theoretical studies calculating energy barriers (E_B)(*29*, *61–65*). Proton transport via a straight perpendicular path through the center of the hexagonal ring in the lattice (left). Proton transport via chemisorption and subsequent bond-flipping through the hexagonal ring (middle). Proton transport via a co-operative mechanism involving multi-protonation (shown here for two protons), where neighboring chemisorbed protons facilitate subsequent protons to first chemisorb on carbon atoms in the hexagonal ring, followed by bond-

flipping via the C-C bond (right). D) Calculated and experimentally measured (red symbols) energy barriers (E_B) for proton transport through pristine graphene, graphene with defects, and pristine h-BN in the literature. Different symbols with the same reference represent distinct material structure including extent of hydrogenation, defects and others. Initial calculations predicted high E_B, but recent studies are exploring transport pathways and mechanisms that allow for lower E_B.

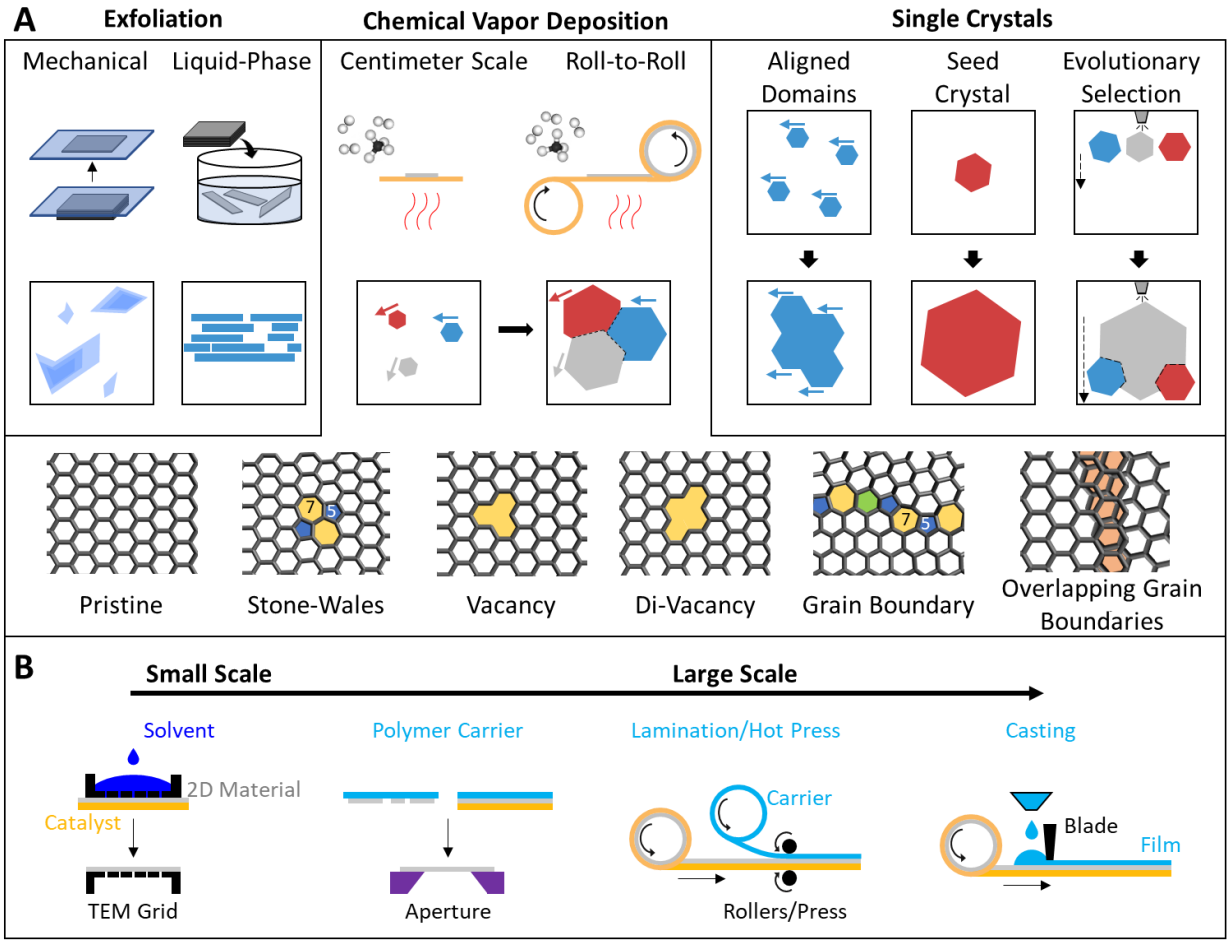

Figure 3. Synthesis and processing of large area atomically thin 2D-materials.

A) Mechanical exfoliation, liquid phase exfoliation and chemical vapor deposition (CVD) represent the main synthesis methods for 2D-materials. Although mechanical exfoliation produces high quality flakes it is not scalable to produce continuous layers. Liquid phase exfoliation allows for scalable synthesis, but realizing atomically thin membranes from flakes produced is challenging. CVD (and its variants) allows for scalable continuous monolayer synthesis including roll-to-roll processes, but the films produced are typically polycrystalline with intrinsic defects such as stone-wales defects, mono and multi-vacancy, and grain boundaries. Efforts to synthesize single crystalline 2D-materials via CVD have focused on *i*) alignment of domains on a single crystalline catalyst/substrate, *ii*) growing a single nucleus larger and *iii*) evolutionary selection where controlled feeding of the fastest growing domain results in it outgrowing others. B) Solvent assisted 2D-material transfer and the use of polymer carrier layers are some of the most commonly used approaches for fabrication of small-area (few microns to centi-meter scale) membranes for applications *e.g.* TEM grids. Large-area (centi-meter to meter scale) energy and separation applications *e.g.* fuel cells isotope separations,

respectively, require the development of scalable approaches such as lamination/hot press and polymer casting.

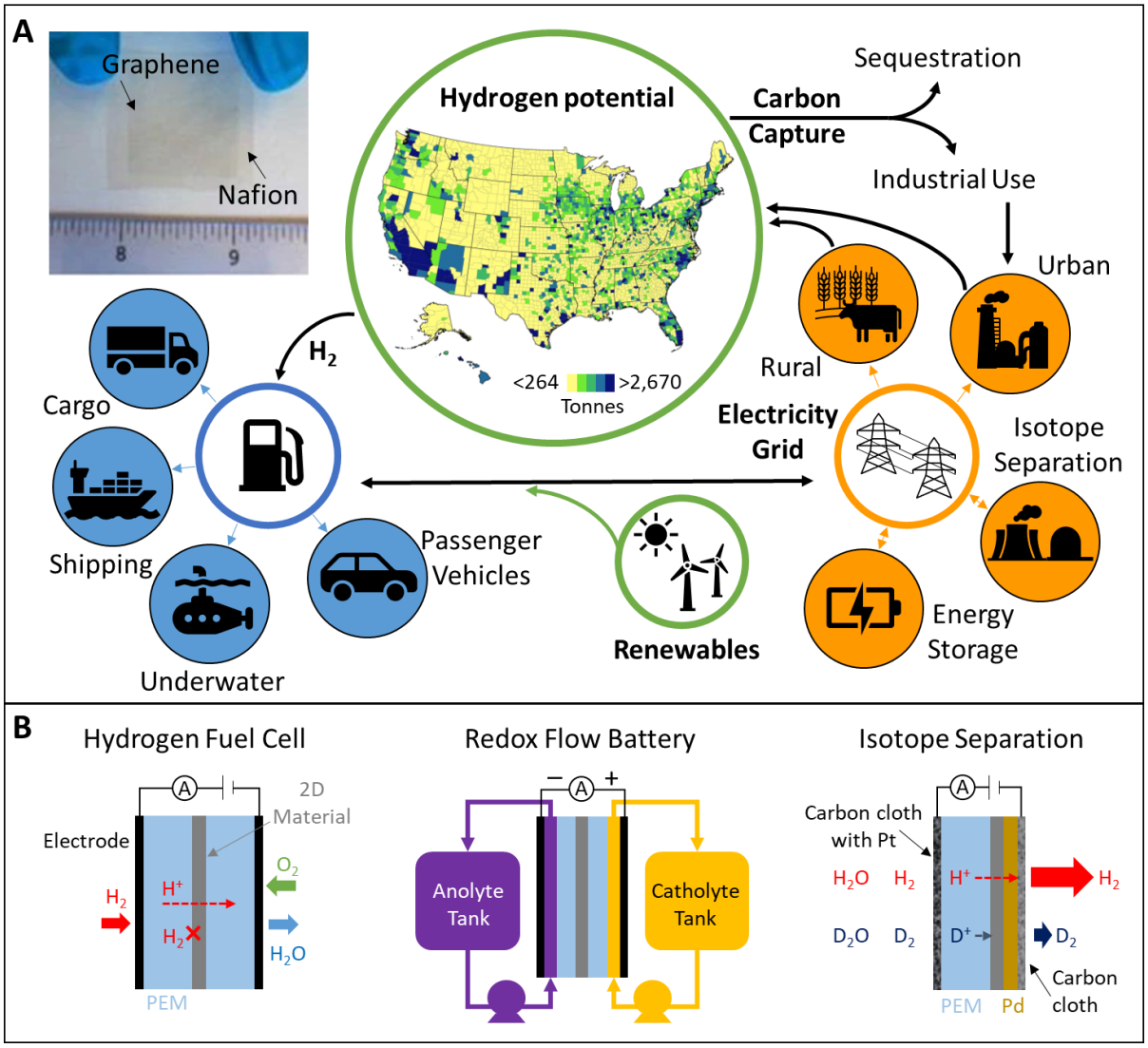

Figure 4. Applications of proton transport through atomically thin membranes.

A) Atomically thin membranes present opportunities to improve efficiency across a wide spectrum of energy generation and conversion processes. Coating a layer of graphene or h-BN onto conventional proton conducting polymers (adapted with permission from Ref. (*67*)) can allow for reduced cross-over and increased efficiency of fuel-cells for transportation and auxiliary power generation, as well as redox flow batteries for grid storage. Electrochemical hydrogen/proton pumps incorporating 2D-materials can allow for compact separators for hydrogen purification and pumping, aiding distributed hydrogen production from rural and urban waste streams. U.S. map showing potential for hydrogen production from biogas generated from waste streams adapted from Ref.(*117*). Atomically thin membranes can allow for hydrogen isotope (H^+/D^+) separation(*67*) and environmental remediation efforts. B) Schematic showing the integration of atomically thin membranes in hydrogen fuel-cells to mitigate cross-over of hydrogen as well as reactants in a redox flow battery while allowing for selective H^+ transport. In

hydrogen fuel cells, H_2 and O_2 are supplied at opposite electrodes. The H_2 dissociates to form H^+ that transport through the membrane and form H_2O as a by-product upon combining with dissociated O_2 and the electrons move via the external circuit. In a redox flow battery, redox ions change oxidation state during charge and discharge cycles via the exchange of H^+ through a membrane and electrons through the external circuit. The use of monolayer graphene and h-BN sandwiched between Nafion in electrochemical proton pumps can enable new approaches for H^+/D^+ separation with separation factor/selectivity ≥8.

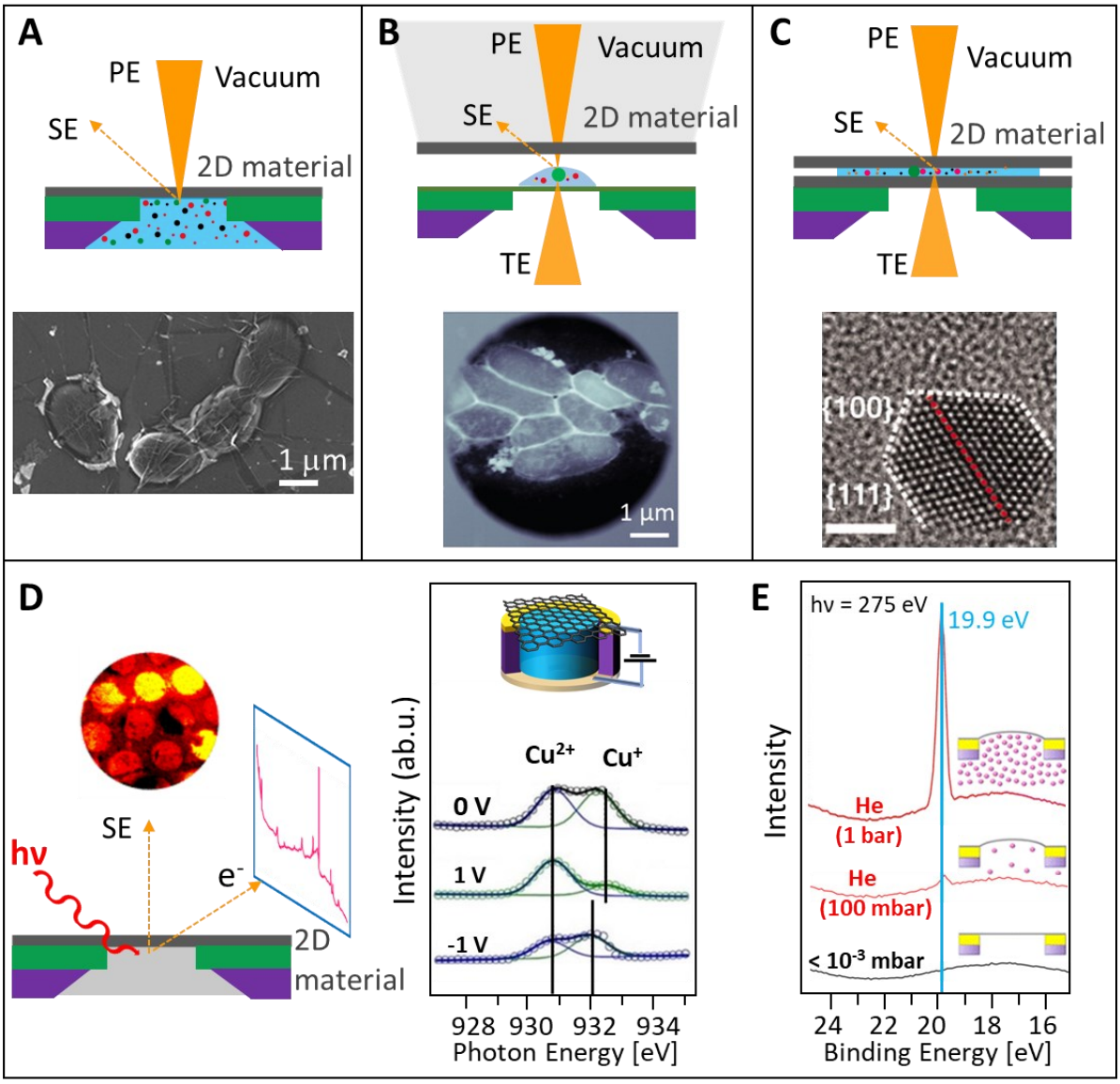

Figure 5. Applications for the electron transparency of atomically thin membranes.

A) Schematic of graphene covering a wet-sample and isolating it from the vacuum environment for scanning electron microscopy (SEM). SEM image of *L*. lactis bacteria using graphene as a veil/covering. (Adapted with permission from Ref.(*138*), scale bar superimposed from the figure provided in the main text.) B) Schematic of graphene membrane sealing the optics in a SEM eliminating the need for a specimen vacuum chamber (airSEM). DF-STEM image of uranium-stained *E*. coli bacteria. (Adapted with permission from Ref.(*131*)). C) Schematic of encapsulated samples between two graphene layers. TEM image of Pt nanoparticle in liquid solution (acquired at 64.22s during growth in solution, scale bar 2nm). (Adapted with permission from Ref.(*97*)). D) Schematic of graphene sealing a gaseous or wet sample for SEM as well as photoelectron spectroscopy and microscopy. Inset shows photoemission electron microscopy (PEEM) image of graphene capped multi-channel array at the O K-edge energy. X-ray absorption spectroscopy (averaged Cu L_3-edge spectra and their Voigt fits) collected on graphene

capped 0.1M $CuSO_4$ solution showing changes in concentration of the mono and bivalent copper ions just below the graphene membrane as a function of its potential. Inset shows a single channel (from the multi-channel array used for PEEM) for clarity. (Adapted with permission from Ref.(*137*)). E) X-ray photoelectron spectra of He (He 1s spectra) collected through single layer graphene membrane capping a reaction cell filled with He gas at different pressures. (Adapted with permission from Ref.(*22*)).